

Lattice simulations with $N_f = 2 + 1$ improved Wilson fermions at a fixed strange quark mass

Gunnar S. Bali,^{1,2,*} Enno E. Scholz,^{1,†} Jakob Simeth,^{1,‡} and Wolfgang Söldner^{1,§}
(RQCD Collaboration)

¹*Institute for Theoretical Physics, University of Regensburg, 93040 Regensburg, Germany*

²*Tata Institute of Fundamental Research, Homi Bhabha Road, Mumbai 400005, India*

(Received 29 June 2016; published 3 October 2016)

The explicit breaking of chiral symmetry of the Wilson fermion action results in additive quark mass renormalization. Moreover, flavor singlet and nonsinglet scalar currents acquire different renormalization constants with respect to continuum regularization schemes. This complicates keeping the renormalized strange quark mass fixed when varying the light quark mass in simulations with $N_f = 2 + 1$ sea quark flavors. Here we present and validate our strategy within the CLS (coordinated lattice simulations) effort to achieve this in simulations with nonperturbatively order- a improved Wilson fermions. We also determine various combinations of renormalization constants and improvement coefficients.

DOI: 10.1103/PhysRevD.94.074501

I. INTRODUCTION

With the gradual removal and reduction of systematic sources of error, including finite volume, unphysical quark mass and lattice spacing effects, lattice QCD simulations have gained prominence in predicting nonperturbative matrix elements that are of phenomenological importance. Present-day large scale simulations employ a multitude of quark actions, namely, overlap and domain wall actions, staggered actions, twisted mass Wilson actions at maximal twist and Wilson actions.

On the one hand overlap and domain wall actions (with a large extent in the fifth direction) have the theoretically most desirable properties, including automatic order- a improvement and an exact chiral symmetry at nonvanishing values of the lattice spacing a . On the other hand Wilson fermions are cheaper to simulate in comparison and no approximations such as the uncontrolled rooting of fermionic determinants are required. Furthermore, unlike in the staggered or twisted mass formulations, no taste or unphysical isospin symmetry breaking takes place: Simulating QCD with $N_f = 2 + 1$ flavors, where we assume the light quarks to be mass-degenerate, there is only one pion mass M_π and one kaon mass M_K .

While in the other fermion formulations mentioned above lattice effects are of order a^2 for most matrix elements, the naive Wilson action has artefacts of order a that need to be removed nonperturbatively, in order to improve the action and operators. Another drawback is additive quark mass renormalization. While in the continuum only for the

axial-vector current a distinction between flavor singlet and nonsinglet dimension three quark bilinears needs to be made, in the Wilson formalism these quark mass combinations (or, equivalently, scalar currents) renormalize differently. In simulations with dynamical sea quarks this complicates parameter tuning within the quark mass plane.

Traditionally, simulations with $N_f = 2 + 1$ (or $N_f = 2 + 1 + 1$) fermions have been performed, keeping the strange quark mass approximately fixed while reducing the light quark mass toward its physical point value. For an overview of simulation points of many lattice collaborations that were available a few years ago, see Fig. 1, taken from Ref. [1]. More details can be found in the reviews [2,3]. For recent simulations see, e.g., Refs. [4–12] ($N_f = 2 + 1$) and [13–15] ($N_f = 2 + 1 + 1$). Determining the point in the quark mass plane where the pion and kaon masses assume their physical values requires knowledge of the lattice spacing. This can only be obtained by extrapolating a third dimensionful observable to this physical

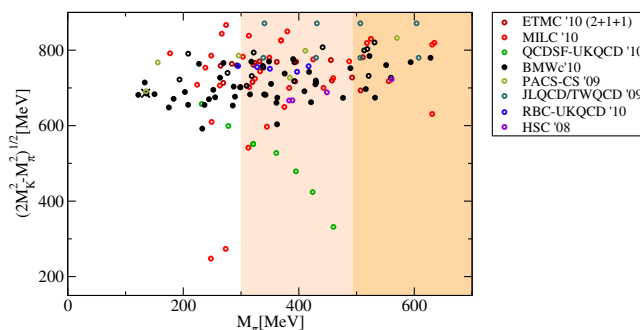


FIG. 1. Positions of some lattice simulations in the quark mass plane, taken from Ref. [1] ($M_\pi \sim \sqrt{m_\ell}$, $(2M_K^2 - M_\pi^2)^{1/2} \sim \sqrt{m_s}$). For details, see also Refs. [2,3].

*gunnar.bali@ur.de

†enno.scholz@ur.de

‡jakob.simeth@ur.de

§wolfgang.soeldner@ur.de

point. Once the scale is known, the initial guesses for the pion and kaon masses may very well turn out to be incorrect. Then new points, e.g., with a different strange quark mass, need to be simulated, or quark mass reweighting becomes necessary.

It was realized by the QCDSF collaboration [4] that extrapolating along a line where the sum of lattice quark masses $m_u + m_d + m_s = 2m_\ell + m_s$ is kept constant (the green outliers in Fig. 1) can be very advantageous, since gluonic observables or the centers of mass of meson and baryon multiplets dominantly depend on the trace of the quark mass matrix but are only mildly affected by the difference $m_s - m_\ell$. This allows for a better controlled approach of the physical point along this mass plane trajectory, with only a small variation of the lattice scale, minimizing the risk of missing the physical point. Therefore, only a very moderate subsequent reweighting of quark masses—if at all—may become necessary. Within the $N_f = 2 + 1$ CLS effort [7] we follow this strategy.

At moderately fine lattice spacings, $a \gtrsim (3 \text{ GeV})^{-1}$, physical point simulations with a spatial extent of the lattice $L > 4/M_\pi$ are possible. However, for complicated observables or at finer lattice spacings, obtaining meaningful physical point results is still prohibitively expensive. In this situation it is desirable to have a second line in the quark mass plane at hand to validate any extrapolation strategy. This has motivated us within the CLS effort to generate ensembles not only at fixed values of $2m_\ell + m_s$ but also to set the renormalized strange quark mass (close) to its physical value while lowering the light quark mass. This additional trajectory allows us to benefit from $SU(2)$ chiral perturbation theory (ChPT) and to determine the corresponding low energy constants. $SU(2)$ ChPT should be more reliable than $SU(3)$ ChPT as the K and the (hypothetical) octet η_8 mesons are not particularly light in nature or in the simulations envisaged here. The additional line in the quark mass plane also provides an alternative to Gell-Mann–Okubo style expansions in the $SU(3)$ flavour symmetry breaking parameter [5,16,17].

Due to the different renormalization patterns of singlet and nonsinglet quark mass combinations, it is not straightforward to keep the renormalized strange quark mass fixed in simulations with Wilson fermions. This is evident from Fig. 1 where no single group managed to keep the renormalized strange quark mass constant, illustrating that even when employing other fermion actions the correct tuning may not be entirely trivial. Here we describe how we achieved an almost constant renormalized strange quark mass, starting from a few existing simulation points with $2m_\ell + m_s = 3m_{\text{symm}} = \text{const}$ and additional points along the $m_s = m_\ell$ line that usually will exist, either from searches for the starting point of the $2m_\ell + m_s = 3m_{\text{symm}}$ trajectory or from nonperturbative renormalization efforts.

This article is organized as follows. In Sec. II we introduce our notations and describe the basic method to

achieve a fixed strange quark mass in our simulations, including order- a improvement. In Sec. III we give a brief overview of the action used and ensembles generated. We then parametrize our quark mass data and also fit previously undetermined improvement coefficients. In Sec. IV we describe our determination of the physical quark mass point. More details on the numerical results and fits are presented in Sec. V, where we also discuss combinations of improvement coefficients, before we conclude in the final section.

II. THE METHOD

We define our notation and derive useful relations, which enable us to relate the strange quark and light quark hopping parameters, defining a line of an (almost) constant renormalized strange quark mass. We then order- a improve this result and discuss how to keep constant renormalized masses of additional valence quark flavors.

A. Definitions and useful relations

We closely follow the notation of Ref. [18], however, substituting $\text{Tr}M = 3\bar{m}$, see below. We assume two mass-degenerate flavors of light sea quarks with masses $m_1 = m_2 = m_\ell$ and one strange sea quark ($m_3 = m_s$). We define κ_{crit} as the hopping parameter value at which the quark mass from the axial Ward-Takahashi identity (AWI mass) in the flavor-symmetric case $m_1 = m_2 = m_3$ vanishes. Lattice quark masses are then defined as¹

$$m_j = \frac{1}{2a} \left(\frac{1}{\kappa_j} - \frac{1}{\kappa_{\text{crit}}} \right). \quad (1)$$

We introduce the following conventions for averages:

$$m_{jk} \equiv \frac{1}{2} (m_j + m_k), \quad (2)$$

$$\bar{m} \equiv \frac{1}{3} (m_s + 2m_\ell), \quad (3)$$

$$\overline{m^2} \equiv \frac{1}{3} (m_s^2 + 2m_\ell^2). \quad (4)$$

We consider flavor nonsinglet ($j \neq k$) pseudoscalar $P^{jk} = \bar{q}^j \gamma_5 q^k$ and axialvector $A_\mu^{jk,0} = \bar{q}^j \gamma_\mu \gamma_5 q^k$ currents. The pseudoscalar current is automatically order- a improved while the improved axial current reads $A_\mu^{jk} = A_\mu^{jk,0} + a c_A \partial_\mu P^{jk}$, where ∂_μ is the symmetrized discrete next neighbor derivative and the improvement coefficient c_A was determined nonperturbatively in Ref. [19]. We define renormalized, order- a improved currents

¹Note that, away from the $m_s = m_\ell$ line, m_ℓ defined in this way can be negative for positive AWI masses. The average mass \bar{m} remains positive.

$$\hat{A}_\mu^{jk} = Z_A A_\mu^{jk} [1 + a(3\bar{b}_A \bar{m} + b_A m_{jk})], \quad (5)$$

$$\hat{P}^{jk} = Z_P P^{jk} [1 + a(3\bar{b}_P \bar{m} + b_P m_{jk})]. \quad (6)$$

Note that Z_P will depend on the target renormalization scheme and scale. The factors of 3 are due to the conventions used for $N_f = 3$ in Ref. [18]. For the action we use, Z_A was calculated in Ref. [20]. Renormalized quark masses can be obtained from the axial Ward identity (AWI)

$$\hat{m}_j + \hat{m}_k = 2\hat{m}_{jk} = \frac{\partial_4 \langle 0 | \hat{A}_4^{jk} | \pi^{jk} \rangle}{\langle 0 | \hat{P}^{jk} | \pi^{jk} \rangle}, \quad (7)$$

where π^{jk} is a pseudoscalar state with quark q^j and antiquark \bar{q}^k .

Finally, we define unrenormalized (but improved) non-singlet AWI masses:

$$\tilde{m}_{jk} = \frac{\partial_4 \langle 0 | A_4^{jk} | \pi^{jk} \rangle}{2 \langle 0 | P^{jk} | \pi^{jk} \rangle}. \quad (8)$$

These can easily be related to the renormalized quark masses via Eqs. (5)–(7). The main CLS ensembles [7] are generated along trajectories of constant average lattice quark masses \bar{m} (and therefore \tilde{m} is constant up to $\mathcal{O}(a)$ corrections). For nonperturbative renormalization purposes we generated additional ensembles along the SU(3) flavor symmetric trajectory, i.e. $m_s = m_\ell$. We now wish to keep \hat{m}_s fixed, varying m_ℓ and adjusting κ_s as required.

The renormalized quark masses can be related to the lattice quark masses:

$$\hat{m}_j = Z_m \{ m_j + (r_m - 1)\bar{m} + a[b_m m_j^2 + 3\bar{b}_m m_j \bar{m} + 3(r_m \bar{d}_m - \bar{b}_m)\bar{m}^2 + (r_m d_m - b_m)\overline{m^2}] \}. \quad (9)$$

At an average quark mass $\bar{m} > 0$ the coupling $g^2 = 6/\beta$ that corresponds to a given lattice spacing a will undergo renormalization too, $g^2 \mapsto \tilde{g}^2 = g^2(1 + b_g a \bar{m})$, where $b_g = 0.012000(2)N_f g^2 + \mathcal{O}(g^4)$ [21]. This means that $Z_J = Z_J[\tilde{g}^2, a(\tilde{g}^2)\mu]$, where we consider $J \in \{m, P, A\}$, and $r_m = r_m[\tilde{g}^2, a(\tilde{g}^2)\mu]$. The dependence on the renormalization scale μ is absent in the case of Z_A , as the nonsinglet axial current does not carry an anomalous dimension. Also the order- a improvement coefficients are functions of \tilde{g}^2 , however, in these cases we can neglect the effect of the difference between g^2 and \tilde{g}^2 , which is of a higher order in a .

Expanding Z_J around g^2 gives

$$\begin{aligned} Z_J[\tilde{g}^2, a(\tilde{g}^2)\mu] &= Z_J[g^2, a(g^2)\mu] \left\{ 1 + \left[\frac{\partial \ln Z_J(g^2, a\mu)}{\partial g^2} \right. \right. \\ &\quad \left. \left. + \frac{d \ln Z_J(g^2, a\mu)}{d \ln a} \frac{\partial \ln a(g^2)}{\partial g^2} \right] g^2 b_g a \bar{m} + \dots \right\} \\ &= Z_J[g^2, a(g^2)\mu] \left\{ 1 + \left[\frac{\partial \ln Z_J(g^2, a\mu)}{\partial g^2} \right. \right. \\ &\quad \left. \left. - \frac{\gamma_J(g^2)}{4\pi\beta(g^2)} \right] g^2 b_g a \bar{m} \right\}, \end{aligned} \quad (10)$$

and similarly for r_m . Note that in this case $d \ln r_m / d \ln a = 0$. The same holds for the scale dependence of Z_A while Z_m carries an anomalous dimension. Above, we have introduced the β -function

$$\beta(g^2) = -\frac{1}{4\pi} \frac{d g^2}{d \ln a} = -\frac{g^2}{2\pi} \left(\beta_0 \frac{g^2}{16\pi^2} + \dots \right), \quad (11)$$

where our normalization convention corresponds to $\beta_0 = 11 - \frac{2}{3}N_f$, and the anomalous dimension of the current (or quark mass) J , which reads

$$\gamma_J(g^2) = \frac{d \ln Z_J}{d \ln a}. \quad (12)$$

We can eliminate b_g by redefining

$$\begin{aligned} \tilde{b}_J(g^2) &\equiv \bar{b}_J(g^2) \\ &\quad + \frac{b_g(g^2)}{N_f} \left[\frac{\partial \ln Z_J(g^2, a\mu)}{\partial g^2} - \frac{\gamma_J(g^2)}{4\pi\beta(g^2)} \right] g^2. \end{aligned} \quad (13)$$

Analogously, the \bar{d}_m improvement coefficient can be replaced by \tilde{d}_m to absorb the effect of b_g on r_m . Note that the anomalous dimension cancels from the above combination. Both \tilde{b}_J and \tilde{d}_m are of $\mathcal{O}(g^4)$ in perturbation theory and at present unknown. With these substitutions Eq. (9) becomes

$$\begin{aligned} \hat{m}_j &= Z_m \{ m_j + (r_m - 1)\bar{m} + a[b_m m_j^2 + 3\tilde{b}_m m_j \bar{m} \\ &\quad + 3(r_m \tilde{d}_m - \tilde{b}_m)\bar{m}^2 + (r_m d_m - b_m)\overline{m^2}] \}, \end{aligned} \quad (14)$$

where Z_m now is a function of g^2 , rather than of \tilde{g}^2 . The only other difference between the two equations is the replacement of the bar-coefficients by tilde-coefficients.

Equation (14) implies that we can reexpress the (unrenormalized) AWI masses in terms of the lattice masses, see Eqs. (48)–(53) of Ref. [18]:

$$\tilde{m}_{jk} = \frac{Z_P Z_m}{Z_A} [m_{jk} + (r_m - 1)\bar{m} + a(\mathcal{A}m_{jk}^2 + 3\mathcal{B}m_{jk}\bar{m} + 9\mathcal{C}\bar{m}^2 + 3\mathcal{D}\bar{m}^2)], \quad (15)$$

where

$$\mathcal{A} = b_P - b_A - 2b_m, \quad (16)$$

$$\mathcal{B} = \tilde{b}_P - \tilde{b}_A + \tilde{b}_m + 2b_m + \frac{1}{3}(r_m - 1)(b_P - b_A), \quad (17)$$

$$\mathcal{C} = \frac{1}{3}[(r_m - 1)(\tilde{b}_P - \tilde{b}_A) + r_m\tilde{d}_m - \tilde{b}_m] - \frac{b_m}{2}, \quad (18)$$

$$\mathcal{D} = \frac{1}{3}\left(r_m d_m + \frac{b_m}{2}\right). \quad (19)$$

Note that we independently verified these results of Ref. [18]. However, we replaced $\tilde{b}_j \mapsto \tilde{b}_j$ and $\tilde{d}_m \mapsto \tilde{d}_m$, absorbing the effect of b_g into these new coefficients. The difference between these two sets of improvement coefficients is of $\mathcal{O}(g^4)$ and is given in Eq. (13). The relation between $N_f = 3$ quark masses $m_j^2 + m_k^2 = -4m_{jk}^2 + 12m_{jk}\bar{m} - 9\bar{m}^2 + 3\bar{m}^2$ was used to derive Eq. (15). For mass-degenerate up and down quarks it will turn out more convenient to rewrite the order- a corrections in terms of their functional dependence on $(m_s - m_\ell)^2$, $(m_s - m_\ell)\bar{m}$ and \bar{m}^2 .

Some of the above improvement coefficients as well as Z_m , Z_P and Z_A have been computed to one-loop order in perturbation theory [22] for the tree-level Symanzik improved gauge action that we use in our simulations²:

$$\begin{aligned} Z &\equiv \frac{Z_m Z_P}{Z_A} = 1 + (0.09546 - 0.11058 + 0.06786)C_F g^2 \\ &= 1 + 0.05274C_F g^2, \end{aligned} \quad (20)$$

$$b_m = d_m = -\frac{1}{2} - 0.05722(5)C_F g^2, \quad (21)$$

$$b_A = 1 + 0.0881(1)C_F g^2, \quad (22)$$

$$b_P = 1 + 0.0890(1)C_F g^2, \quad (23)$$

where $C_F = 4/3$ and terms of $\mathcal{O}(g^4)$ are ignored. This means the difference $b_A - b_P$ practically vanishes to $\mathcal{O}(g^2)$ while $\tilde{b}_A - \tilde{b}_P$, being a sea quark effect, exactly vanishes to

²For the Z_j we quote the more precise values given in Ref. [23], using $c_{SW} = 1$, which is consistent to this order. The ordering of the numerical values in the first line corresponds to $Z_m = Z_S^{-1}$, Z_P and Z_A^{-1} , where Z_m and Z_P are the conversions to the $\overline{\text{MS}}$ scheme at the scale $\mu = a^{-1}$. The scale and scheme dependence cancels from the combination Z .

this order. Therefore, keeping the renormalized strange quark mass \hat{m}_s constant amounts to keeping the AWI mass

$$\begin{aligned} \tilde{m}_s &\equiv 2\tilde{m}_{13} - \tilde{m}_{12} \\ &= \hat{m}_s \frac{Z_P}{Z_A} \{1 + a[3(\tilde{b}_P - \tilde{b}_A)\bar{m} + (b_P - b_A)m_s]\} \end{aligned} \quad (24)$$

fixed, up to $\mathcal{O}(g^4 a \bar{m})$ and $\mathcal{O}(g^2 a m_s)$ corrections with small coefficients. It has been confirmed nonperturbatively [24] that the $a m_s$ term is not unnaturally large. In the absence of other information from nonperturbative approaches, in particular on $\tilde{b}_A - \tilde{b}_P$, we will keep \tilde{m}_s fixed instead of \hat{m}_s .

We remark that for the gauge and fermion action that we use r_m has been computed perturbatively [25], with the result

$$r_m = 1 + 0.001158(1)C_F N_f g^4. \quad (25)$$

From our study we will see that the nonperturbative values are much larger.

Differences of AWI quark masses are related by the nonsinglet renormalization constant Z of Eq. (20) to differences of the above lattice quark masses while the average AWI quark mass \bar{m} is related by $Z r_m$ to the average lattice quark mass [18,26–28]. Below we will make use of the relations

$$\begin{aligned} 2(m_{13}^2 - m_{12}^2) &= \frac{1}{2}(m_s + m_\ell)^2 - 2m_\ell^2 \\ &= -\frac{1}{6}(m_s - m_\ell)^2 + 2(m_s - m_\ell)\bar{m}, \end{aligned} \quad (26)$$

$$\bar{m}^2 = \bar{m}^2 + \frac{2}{9}(m_s - m_\ell)^2. \quad (27)$$

Differences and sums of AWI masses read:

$$\begin{aligned} \tilde{m}_s - \tilde{m}_\ell &= 2(\tilde{m}_{13} - \tilde{m}_{12}) \\ &= Z \left\{ (m_s - m_\ell) + a \left[-\frac{\mathcal{A}}{6}(m_s - m_\ell)^2 \right. \right. \\ &\quad \left. \left. + (2\mathcal{A} + 3\mathcal{B})(m_s - m_\ell)\bar{m} \right] \right\}, \end{aligned} \quad (28)$$

$$\begin{aligned} \bar{m} &= \frac{1}{3}(\tilde{m}_{12} + \tilde{m}_{23} + \tilde{m}_{31}) = \frac{1}{3}(\tilde{m}_s + 2\tilde{m}_\ell) \\ &= Z \left\{ r_m \bar{m} + a \left[\frac{1}{18}(\mathcal{A} + 12\mathcal{D})(m_s - m_\ell)^2 \right. \right. \\ &\quad \left. \left. + (\mathcal{A} + 3\mathcal{B} + 9\mathcal{C} + 3\mathcal{D})\bar{m}^2 \right] \right\}, \end{aligned} \quad (29)$$

where $\tilde{m}_\ell \equiv \tilde{m}_{12}$, assuming $\kappa_1 = \kappa_2$. Having rewritten everything in terms of differences of quark masses and

average quark masses, we can reexpress the improvement terms through AWI masses, which will allow us to eliminate κ_{crit} from most equations:

$$\tilde{m}_s - \tilde{m}_\ell = Z(m_s - m_\ell) - \frac{a}{Z} \left[\frac{\mathcal{A}}{6} (\tilde{m}_s - \tilde{m}_\ell)^2 + \frac{\mathcal{B}_0}{r_m} \tilde{m} (\tilde{m}_s - \tilde{m}_\ell) \right], \quad (30)$$

$$\tilde{m} = Zr_m \bar{m} - \frac{a}{Z} \left[\frac{\mathcal{C}_0 r_m}{9} (\tilde{m}_s - \tilde{m}_\ell)^2 + \frac{\mathcal{D}_0}{2r_m} \tilde{m}^2 \right], \quad (31)$$

where we substituted the combinations \mathcal{B}, \dots by \mathcal{B}_0, \dots , that are normalized such that $\mathcal{A} = \mathcal{B}_0 = \mathcal{C}_0 = \mathcal{D}_0 = 1$ at tree-level:

$$\begin{aligned} \mathcal{B}_0 &= -2\mathcal{A} - 3\mathcal{B} \\ &= -(r_m + 1)(b_P - b_A) - 2b_m - 3(\tilde{b}_P - \tilde{b}_A + \tilde{b}_m), \end{aligned} \quad (32)$$

$$\begin{aligned} \mathcal{C}_0 &= -\frac{1}{2r_m} (\mathcal{A} + 12\mathcal{D}) \\ &= -\frac{1}{2r_m} (b_P - b_A) - 2d_m, \end{aligned} \quad (33)$$

$$\begin{aligned} \mathcal{D}_0 &= -\frac{2}{r_m} (\mathcal{A} + 3\mathcal{B} + 9\mathcal{C} + 3\mathcal{D}) \\ &= -2(b_P - b_A + d_m) - 6(\tilde{b}_P - \tilde{b}_A + \tilde{d}_m). \end{aligned} \quad (34)$$

We also made the r_m -dependence explicit since this, though formally $1 + \mathcal{O}(g^4)$ [see Eq. (25)], will turn out significantly larger than one. Note that $d_m = b_m + \mathcal{O}(g^4) = -1/2 + \mathcal{O}(g^2)$ and $b_P = b_A + \mathcal{O}(g^2) = 1 + \mathcal{O}(g^2)$ [see Eqs. (20)–(23)] while all improvement coefficients \tilde{d}_J and \tilde{b}_J only receive contributions at $\mathcal{O}(g^4)$.

Although not needed here, for completeness we also express lattice quark mass combinations through AWI masses:

$$\begin{aligned} m_s - m_\ell &= \frac{1}{2a} \left(\frac{1}{\kappa_s} - \frac{1}{\kappa_\ell} \right) \\ &= \frac{\tilde{m}_s - \tilde{m}_\ell}{Z} \left\{ 1 + a \left[\frac{\mathcal{A}}{6Z} (\tilde{m}_s - \tilde{m}_\ell) + \frac{\mathcal{B}_0}{Zr_m} \tilde{m} \right] \right\}, \end{aligned} \quad (35)$$

$$\begin{aligned} \bar{m} &= \frac{1}{6a} \left(\frac{1}{\kappa_s} + \frac{2}{\kappa_\ell} - \frac{3}{\kappa_{\text{crit}}} \right) \\ &= \frac{\tilde{m}}{Zr_m} \left\{ 1 + a \left[\frac{\mathcal{C}_0 Z r_m}{9Z^2} \frac{(\tilde{m}_s - \tilde{m}_\ell)^2}{\tilde{m}} + \frac{\mathcal{D}_0}{2Zr_m} \tilde{m} \right] \right\}. \end{aligned} \quad (36)$$

B. Leading order determination of the target κ_s and κ_ℓ parameters

We need to predict how we have to adjust κ_s as a function of $\kappa_\ell < \kappa_{\ell,\text{ph}}$ to keep $\tilde{m}_s = \tilde{m}_{s,\text{ph}}$ fixed (and therefore the renormalized strange quark mass \hat{m}_s approximately constant). We assume that the parameters $\kappa_{\ell,\text{ph}}$ and $\kappa_{s,\text{ph}}$ that correspond to the physical point have already been determined, see Sec. IV. Neglecting $\mathcal{O}(am)$ terms, we can write

$$\begin{aligned} 3\tilde{m}_s &= 2(\tilde{m}_s - \tilde{m}_\ell) + 3\tilde{m} \\ &= \frac{Z}{2a} \left[2 \left(\frac{1}{\kappa_s} - \frac{1}{\kappa_\ell} \right) + r_m \left(\frac{1}{\kappa_s} + \frac{2}{\kappa_\ell} - \frac{3}{\kappa_{\text{crit}}} \right) \right], \end{aligned} \quad (37)$$

where we keep the left-hand side constant. Solving $\tilde{m}_s = \tilde{m}_{s,\text{ph}}$ for $1/\kappa_s$ gives

$$\frac{1}{\kappa_s} = \frac{2}{2 + r_m} \left(\frac{3a}{Z} \tilde{m}_{s,\text{ph}} + (1 - r_m) \frac{1}{\kappa_\ell} + \frac{3r_m}{2} \frac{1}{\kappa_{\text{crit}}} \right). \quad (38)$$

κ_{crit} and $\tilde{m}_{s,\text{ph}}$ can be eliminated by subtracting the result at the physical point from both sides of this equation:

$$\frac{1}{\kappa_s} = \frac{1}{\kappa_{s,\text{ph}}} + \frac{2(1 - r_m)}{2 + r_m} \left(\frac{1}{\kappa_\ell} - \frac{1}{\kappa_{\ell,\text{ph}}} \right), \quad (39)$$

i.e. for predicting the target κ_s as a function of κ_ℓ , up to $\mathcal{O}(a)$ corrections, we only need to know the value of the parameter r_m , in addition to determining the physical point. Note that $r_m > 1$, which means that as we decrease κ_ℓ away from the physical point, we have to increase κ_s .

The equality $3\tilde{m}_\ell = (\tilde{m}_\ell - \tilde{m}_s) + 3\tilde{m}$ results in the relation

$$3\tilde{m}_\ell = \frac{Z}{2a} \left(\frac{r_m - 1}{\kappa_s} + \frac{2r_m + 1}{\kappa_\ell} - \frac{3r_m}{\kappa_{\text{crit}}} \right), \quad (40)$$

in analogy to Eq. (37). We can again eliminate κ_{crit} , by subtracting the result at the physical point. Furthermore, we substitute the difference $\kappa_s^{-1} - \kappa_{s,\text{ph}}^{-1}$ of Eq. (39), giving

$$a(\tilde{m}_\ell - \tilde{m}_{\ell,\text{ph}}) = \frac{Z}{2} \frac{3r_m}{2 + r_m} \left(\frac{1}{\kappa_\ell} - \frac{1}{\kappa_{\ell,\text{ph}}} \right). \quad (41)$$

If we are now targeting a value $\tilde{m}_\ell \neq \tilde{m}_{\ell,\text{ph}}$, we can extract the corresponding shift in κ_ℓ^{-1} relative to the physical point from the above equation.

C. Order- a improvement

Here we show how to order- a improve Eq. (39). However, we refrain from working out the equivalent expression for the light quark mass shift Eq. (41) as for our purposes an approximate determination of the target κ_ℓ value is sufficient. Above we have not only related AWI

masses to lattice masses, introducing Z and r_m , but also improvement terms with coefficients \mathcal{A} , \mathcal{B}_0 , \mathcal{C}_0 and \mathcal{D}_0 have been worked out.

Multiplying Eq. (30) by two and Eq. (31) by three, it is easy to derive an order- a improved version of Eq. (37):

$$3\tilde{m}_s = \frac{Z}{a} \left(\frac{2+r_m}{2\kappa_s} + \frac{r_m-1}{\kappa_\ell} - \frac{3r_m}{2\kappa_{\text{crit}}} \right) - \frac{a}{3Z} \left[(\mathcal{A} + \mathcal{C}_0 r_m)(\tilde{m}_s - \tilde{m}_\ell)^2 + \frac{6\mathcal{B}_0}{r_m}(\tilde{m}_s - \tilde{m}_\ell)\tilde{m} + \frac{9\mathcal{D}_0}{2r_m}\tilde{m}^2 \right]. \quad (42)$$

Next we keep $\tilde{m}_s \equiv \tilde{m}_s(\kappa_\ell, \kappa_s) = \tilde{m}_{s,\text{ph}}$ fixed and compute differences between simulated and physical mass values:

$$(\tilde{m}_s - \tilde{m}_\ell)^2 - (\tilde{m}_s - \tilde{m}_{\ell,\text{ph}})^2 = \frac{Z}{2a} \left(\frac{1}{\kappa_\ell} - \frac{1}{\kappa_{\ell,\text{ph}}} \right) (\tilde{m}_\ell + \tilde{m}_{\ell,\text{ph}} - 2\tilde{m}_s), \quad (43)$$

$$(\tilde{m}_s - \tilde{m}_\ell)\tilde{m} - (\tilde{m}_s - \tilde{m}_{\ell,\text{ph}})\tilde{m}_{\text{ph}} = \frac{Z}{6a} \left(\frac{1}{\kappa_\ell} - \frac{1}{\kappa_{\ell,\text{ph}}} \right) [\tilde{m}_s - 2(\tilde{m}_\ell + \tilde{m}_{\ell,\text{ph}})], \quad (44)$$

$$\tilde{m}^2 - \tilde{m}_{\text{ph}}^2 = \frac{2Z}{9a} \left(\frac{1}{\kappa_\ell} - \frac{1}{\kappa_{\ell,\text{ph}}} \right) (\tilde{m}_s + \tilde{m}_\ell + \tilde{m}_{\ell,\text{ph}}). \quad (45)$$

Above we have reexpressed the nonsinglet combination $\tilde{m}_\ell - \tilde{m}_{\ell,\text{ph}}$ through differences of inverse hopping parameters. We now isolate $1/\kappa_s$ in Eq. (42) and subtract the physical point values from both sides of the resulting equation:

$$\frac{1}{\kappa_s} - \frac{1}{\kappa_{s,\text{ph}}} = \frac{2}{2+r_m} \left(\frac{1}{\kappa_\ell} - \frac{1}{\kappa_{\ell,\text{ph}}} \right) \left\{ 1 - r_m + \frac{a}{6Z} \left[(\mathcal{A} + \mathcal{C}_0 r_m)(-2\tilde{m}_{s,\text{ph}} + \tilde{m}_{\ell,\text{ph}} + \tilde{m}_\ell) + \frac{2\mathcal{B}_0}{r_m}(\tilde{m}_{s,\text{ph}} - 2(\tilde{m}_{\ell,\text{ph}} + \tilde{m}_\ell)) + \frac{2\mathcal{D}_0}{r_m}(\tilde{m}_{s,\text{ph}} + \tilde{m}_{\ell,\text{ph}} + \tilde{m}_\ell) \right] \right\}. \quad (46)$$

Using Eq. (41), we can reexpress \tilde{m}_ℓ above in terms of κ_ℓ , $\kappa_{\ell,\text{ph}}$ and $\tilde{m}_{\ell,\text{ph}}$. This gives

$$\frac{1}{\kappa_s} = \frac{1}{\kappa_{s,\text{ph}}} + \frac{2}{3}x \left\{ 1 - r_m + \frac{1}{3} \left[\frac{\mathcal{B}_0 + \mathcal{D}_0}{r_m} - (\mathcal{A} + \mathcal{C}_0 r_m) \right] \times \frac{a\tilde{m}_{s,\text{ph}}}{Z} + \frac{1}{3} \left(\mathcal{A} + \mathcal{C}_0 r_m + \frac{2\mathcal{D}_0 - 4\mathcal{B}_0}{r_m} \right) \times \left(\frac{a\tilde{m}_{\ell,\text{ph}}}{Z} + \frac{r_m}{4}x \right) \right\}, \quad (47)$$

where

$$x = \frac{3}{2+r_m} \left(\frac{1}{\kappa_\ell} - \frac{1}{\kappa_{\ell,\text{ph}}} \right). \quad (48)$$

We employ Eq. (47) to determine the order- a improved value of κ_s . The last term of this equation is numerically subleading since $\tilde{m}_{\ell,\text{ph}} \approx 0$ and terms quadratic in x can be neglected too as long as $\tilde{m}_\ell \ll \tilde{m}_s$. Therefore, the dominant order- a correction amounts to a constant shift of κ_s^{-1} , relative to Eq. (39). Note that at tree-level $r_m = \mathcal{A} = \mathcal{B}_0 = \mathcal{C}_0 = \mathcal{D}_0 = 1$ and therefore, $\kappa_s = \text{const.}$, as it should be in the noninteracting case.

D. Comment on additional valence quark flavors

We now consider the partially quenched situation, introducing additional ‘‘charm’’ valence quarks of the lattice mass

$$m_c = m_4 = m_5 = \frac{1}{2a} \left(\frac{1}{\kappa_c} - \frac{1}{\kappa_{\text{crit}}} \right), \quad (49)$$

where κ_{crit} is still the hopping parameter for the $N_f = 3$ case at vanishing quark masses. Again, one can obtain the AWI charm quark mass from Eq. (7). As the charm quark is quenched, rather than using the currents \hat{A}_μ^{4j} and \hat{P}^{4j} with $j \in \{1, 2, 3\}$, we can also just compute \hat{A}_μ^{45} and \hat{P}^{45} , pretending we have two distinct (but mass-degenerate) charm quark flavors. In this partially quenched situation, rather than working with the flavor symmetry group $\text{SU}(3)$, we have to work with the graded group $\text{SU}(5|2)$, replacing mass traces in Eq. (14) by supertraces. The changes can be worked out easily and reduce to the preceding formulas when replacing the flavor combination 45 by 12 and m_c by m_ℓ . In particular we have

$$\tilde{m}_c = \frac{Z_P}{Z_A} \hat{m}_c \{ 1 + a[(b_P - b_A)m_c + 3(\tilde{b}_P - \tilde{b}_A)\tilde{m}] \}, \quad (50)$$

where

$$\hat{m}_c = \frac{\partial_4 \langle 0 | \hat{A}_4^{45} | \pi^{45} \rangle}{2 \langle 0 | \hat{P}^{45} | \pi^{45} \rangle}. \quad (51)$$

Note that \tilde{m} above still denotes the mass average over the three sea quark flavors only.

Expressing the renormalized charm quark mass through lattice quark masses, we obtain the following relation between the AWI charm mass and partially quenched lattice quark masses:

$$\begin{aligned} \tilde{m}_c = & Z\{m_c + (r_m - 1)\bar{m} + a[(\mathcal{A} + 3b_m)m_c^2 \\ & - (\mathcal{B}_0 + 2\mathcal{A} + 6b_m)\bar{m}m_c \\ & - \frac{1}{18}(2r_m\mathcal{C}_0 + \mathcal{A} + 6b_m)(m_s - m_\ell)^2 \\ & - \frac{1}{2}(r_m\mathcal{D}_0 - 2\mathcal{A} - 2\mathcal{B}_0 - 6b_m)\bar{m}^2]\}. \end{aligned} \quad (52)$$

In spite of the fact that the charm quark is quenched, r_m still appears in the above equation since we defined the lattice quark mass relative to the inverse sea quark critical hopping parameter.³

It is now clear how to keep the AWI (or the renormalized) charm quark mass approximately constant:

$$\tilde{m}_c - \bar{m} = Z(m_c - \bar{m})[1 + \mathcal{O}(a)]. \quad (53)$$

In the situation $\bar{m} = m_{\text{symm}}$, unsurprisingly, at least up to order- a effects, m_c (and therefore κ_c) should be kept constant. One may wonder if, owing to the heavy charm quark mass, discretization effects may be substantial. Examining Eq. (59) we notice that as long as \bar{m} is kept constant only the parametrically small second last term ($m_s - m_\ell \ll m_{c,\text{ph}}$) changes. Therefore, along the $\bar{m} = m_{\text{symm}}$ trajectory, also keeping track of the dominant order- a effects, m_c , i.e. κ_c , should remain constant.

In Secs. II B and II C we worked out how κ_s has to be varied to keep $\tilde{m}_s = \tilde{m}_{s,\text{ph}}$ constant. What happens along this line? In this case

$$\tilde{m}_{c,\text{ph}} - \tilde{m}_{s,\text{ph}} = Z(m_c - m_s)[1 + \mathcal{O}(a)] \quad (54)$$

should remain constant. This means that in this situation the difference between $1/\kappa_c$ and $1/\kappa_s$ should be kept approximately fixed, too:

$$\frac{1}{\kappa_c} = \frac{1}{\kappa_s} + \frac{1}{\kappa_{c,\text{ph}}} - \frac{1}{\kappa_{s,\text{ph}}}. \quad (55)$$

The order- a contributions are again captured by Eq. (59) and the compensation term can be worked out if needed, in analogy to the discussion of Sec. II C above.

III. SIMULATION PARAMETERS AND FIT PROCEDURE

In this article we present results obtained at two β values: $\beta = 3.4$, corresponding to $a \approx 0.085$ fm, and $\beta = 3.55$ ($a \approx 0.064$ fm). Investigations at further lattice spacings are in progress. At each lattice spacing the simulations cover four mass points ranging from a pion mass

³Note that when setting $\tilde{m}_c = \tilde{m}_\ell$ and $m_c = m_\ell$, substituting $m_\ell^2 = \bar{m}^2 - \frac{2}{3}\bar{m}(m_s - m_\ell) + \frac{1}{9}(m_s - m_\ell)^2$ and $\bar{m}m_\ell = \bar{m}^2 - \frac{1}{3}\bar{m}(m_s - m_\ell)$, Eq. (59) reduces to the unquenched case discussed previously, as it should.

$M_\pi \approx 200$ MeV up to $M_\pi \approx 420$ MeV along the $\bar{m} = m_{\text{symm}} = \text{const}$ line with $M_\pi L > 4$ (3.9 in one case). At $\beta = 3.4$ one additional point exists along this line at $M_\pi \approx 129$ MeV (D100). However, as in this case we have only limited statistics and $M_\pi L < 4$, we will discard this ensemble from any fit. For an overview of the analyzed ensembles, see Table I. The lattice spacing and meson mass estimates are based on the continuum limit value of the scale [29] $\sqrt{8t_0} = 0.4144(59)(37)$ fm that was obtained by the BMW Collaboration [30]. We utilize open boundary conditions in time [31], with the exception of the rqed017, rqed019, rqed021, B250, X250 and X251 ensembles, which are periodic in time for gauge fields and antiperiodic for fermions. Note that the ensembles under investigation correspond to lattice spacings at which topological freezing is not yet a major problem [7], enabling us to use (anti) periodic boundary conditions. We remark that at $\beta = 3.55$ and $\kappa_\ell = \kappa_s = 0.137$ there exist two ensembles, H200 and N202, both with $LM_\pi > 4$. However, in the first case $L \approx 2$ fm is rather small in physical units. While this does not appear to affect the AWI mass, the measured pion mass on the larger volume comes out somewhat lighter. Therefore, we discard H200 from further analysis.

In addition to the already existing $\bar{m} = m_{\text{symm}}$ point at $m_s = m_\ell$, we first generated three other points along the flavor symmetric line for both lattice spacings, one at a bigger and two at smaller values of the quark mass. The data along these two lines in the quark mass plane enabled us to estimate Z , r_m and κ_{crit} from fits of the form [see Eqs. (30) and (31)]:

$$\begin{aligned} a\tilde{m}_s - a\tilde{m}_\ell = & \frac{Z}{2} \left(\frac{1}{\kappa_s} - \frac{1}{\kappa_\ell} \right) \\ & \times \left[1 - \frac{\mathcal{A}}{12} \left(\frac{1}{\kappa_s} - \frac{1}{\kappa_\ell} \right) - \mathcal{B}_0 a\bar{m} \right], \end{aligned} \quad (56)$$

$$a\bar{m} = Zr_m \left[a\bar{m} - \frac{\mathcal{C}_0}{36} \left(\frac{1}{\kappa_s} - \frac{1}{\kappa_\ell} \right)^2 - \frac{\mathcal{D}_0}{2} (a\bar{m})^2 \right]. \quad (57)$$

The combination $a\bar{m} = (2\kappa_\ell^{-1} + \kappa_s^{-1} - 3\kappa_{\text{crit}}^{-1})/6$ above depends on κ_{crit} . To this order in a this parameter can in principle be substituted by the measured value of $a\tilde{m}/(Zr_m)$ if desired. This is possible because we will neither need the value of κ_{crit} for our determination of the physical point nor for predicting the κ_s trajectory (as a function of κ_ℓ) along which $\tilde{m}_s \approx (Z_P/Z_A)\hat{m}_s$ is kept fixed, see Eqs. (39) and (47).

We were unable to reliably fit seven (or six) parameters to data from seven ensembles, covering just the $\bar{m} = m_{\text{symm}}$ and $m_s = m_\ell$ lines. Moreover, \mathcal{D}_0 is insensitive to the $\bar{m} = m_{\text{symm}}$ points, \mathcal{A} does not depend on the $m_s = m_\ell$ points and a determination of \mathcal{B}_0 requires points at additional positions in the quark mass plane. Therefore, we initially made use of the one-loop estimates

TABLE I. Analyzed CLS (and RQCD) ensembles at $\beta = 3.4$ and $\beta = 3.55$: mass plane trajectory ($\bar{m} = m_{\text{symm}}$, $m_s = m_\ell$ or $\tilde{m}_s = \tilde{m}_{s,\text{ph}}$), ensemble name, hopping parameter values, linear extent in terms of the inverse pion mass, number of lattice points, $\sqrt{8t_0}/a$, estimates of pion and kaon masses from assigning $\sqrt{8t_{0,\text{ph}}} = 0.4144(70)$ fm [30] (also the lattice spacings a are estimated in this way), the AWI quark masses in lattice units and the number of molecular dynamics units N_{MD} . In most cases the trajectory length is two and measurements are taken every four units. We complement the $\sqrt{8t_0}/a$ values determined in Ref. [7] by preliminary estimates obtained on the newly generated ensembles. Note that the ensembles H101, H200 and N202 are at the same time on the $\bar{m} = m_{\text{symm}}$ and $m_s = m_\ell$ lines. All D100 results are very preliminary due to insufficient statistics. We exclude D100, H200 and rqcd019 from further analysis. Preliminary results are typeset in *Italics*.

Trajectory	Ensemble	κ_ℓ	κ_s	LM_π	N_t	N_s^3	$\sqrt{8t_0}/a$	$\frac{M_\pi}{\text{MeV}}$	$\frac{M_K}{\text{MeV}}$	$a\tilde{m}_\ell$	$a\tilde{m}_s$	N_{MD}
$\beta = 3.4$ [$a = 0.0854(15)$ fm]												
$\bar{m} = m_{\text{symm}}$	H101	0.13675962	0.13675962	5.8	96	32 ³	4.772(5)	422	422	0.009201(39)	0.009201(39)	8000
	H102	0.136865	0.136549339	4.9	96	32 ³	4.800(6)	356	442	0.006502(46)	0.013836(43)	7988
	H105	0.13697	0.13634079	3.9	96	32 ³	4.819(6)	282	467	0.003951(52)	0.018672(52)	11332
	C101	0.13703	0.136222041	4.6	96	48 ³	4.824(4)	223	476	0.002466(32)	0.021242(34)	6208
	D100	0.13709	0.136103607	3.2	128	64 ³	<i>4.860(4)</i>	129	482	0.000801(30)	0.023552(43)	492
$m_s = m_\ell$	rqcd019	0.1366	0.1366	8.4	32	32 ³	<i>4.454(5)</i>	607	607	0.018094(77)	0.018094(77)	1686
	rqcd021	0.136813	0.136813	4.7	32	32 ³	<i>4.925(12)</i>	340	340	0.005983(63)	0.005983(63)	1541
	rqcd017	0.136865	0.136865	3.3	32	32 ³	<i>5.100(7)</i>	238	238	0.002799(92)	0.002799(92)	1849
$\tilde{m}_s = \tilde{m}_{s,\text{ph}}$	H107	0.136945665908	0.136203165143	5.1	96	32 ³	<i>4.665(6)</i>	368	549	0.006662(50)	0.023981(60)	6256
	H106	0.137015570024	0.136148704478	3.8	96	32 ³	<i>4.751(6)</i>	272	519	0.003775(70)	0.024029(68)	6212
	C102	0.1370508458	0.136129062556	4.6	96	48 ³	<i>4.790(4)</i>	223	504	0.002467(34)	0.023956(54)	6000
$\beta = 3.55$ [$a = 0.0644(11)$ fm]												
$\bar{m} = m_{\text{symm}}$	H200	0.137	0.137	4.4	96	32 ³	6.419(14)	418	418	0.006865(22)	0.006865(22)	8000
	N202	0.137	0.137	6.4	128	48 ³	<i>6.427(6)</i>	410	410	0.006854(16)	0.006854(16)	3536
	N203	0.13708	0.136840284	5.4	128	48 ³	<i>6.416(4)</i>	345	441	0.004738(15)	0.011047(12)	6172
	N200	0.13714	0.13672086	4.4	128	48 ³	6.424(5)	283	461	0.003164(12)	0.014132(11)	6800
	D200	0.1372	0.136601748	4.2	128	64 ³	6.430(4)	199	479	0.001538(10)	0.017229(12)	4000
$m_s = m_\ell$	B250	0.1367	0.1367	7.4	64	32 ³	<i>5.873(8)</i>	706	706	0.018772(39)	0.018772(39)	1776
	X250	0.13705	0.13705	5.4	64	48 ³	<i>6.500(8)</i>	347	347	0.004899(21)	0.004899(21)	1380
	X251	0.1371	0.1371	4.2	64	48 ³	<i>6.623(9)</i>	268	268	0.002895(25)	0.002895(25)	1384
	N204	0.137112	0.136575049	5.5	128	48 ³	<i>6.290(5)</i>	352	545	0.004822(14)	0.018927(15)	3692
$\tilde{m}_s = \tilde{m}_{s,\text{ph}}$	N201	0.13715968	0.136561319	4.5	128	48 ³	<i>6.351(4)</i>	284	522	0.003146(14)	0.018849(15)	6000
	D201	0.137207	0.136546436	4.1	128	64 ³	<i>6.409(4)</i>	198	499	0.001552(16)	0.018874(17)	4312

$$\mathcal{A} = 1 + 0.1153(2)C_F g^2, \quad (58)$$

$$\mathcal{B}_0 = \mathcal{D}_0 = 1 + 0.1126(3)C_F g^2, \quad (59)$$

$$\mathcal{C}_0 = 1 + 0.1140(1)C_F g^2, \quad (60)$$

see Eqs. (16), (21)–(23) and (32)–(34). After investigating various fits with different combinations of \mathcal{A} , \mathcal{C}_0 and \mathcal{D}_0 as free parameters, we found that fixing \mathcal{A} , \mathcal{B}_0 and \mathcal{D}_0 to the above one-loop estimates but allowing \mathcal{C}_0 to float gave a good and stable description of the data. Note that the nonperturbatively determined values of \mathcal{A} [24] were not available at the beginning of this study. This then enabled us to predict the κ_s values that corresponded to our target AWI strange quark mass (see Sec. IV below), using Eq. (47). Table I demonstrates that indeed we managed to keep the AWI strange quark mass \tilde{m}_s constant in simulations with Wilson fermions within statistical errors of 0.3% and 0.1% at $\beta = 3.4$ and $\beta = 3.55$, respectively, see also Fig. 5 below.

After simulating three additional points along the $\tilde{m}_s = \tilde{m}_{s,\text{ph}} = \text{const}$ trajectory for each lattice spacing, we used the nonperturbative values $\mathcal{A} = 2.91(33)$ and $\mathcal{A} = 2.27(14)$ for $\beta = 3.4$ and $\beta = 3.55$, respectively, that were obtained employing coordinate space methods [24], to determine the remaining six parameters from a combined correlated fit to all data. Varying \mathcal{A} within its uncertainty [24] had only a very insignificant impact on the remaining six fit parameters. After excluding the rather heavy (in lattice units) $\beta = 3.4$ rqcd019 point from the fit, we have nine and ten ensembles with 15 and 16 different quark mass values at our disposal at $\beta = 3.4$ and $\beta = 3.55$, respectively.

The resulting fit parameters are shown in Table II. The data only mildly constrain the parameter \mathcal{D}_0 , which comes out to be compatible with zero within large errors. r_m , \mathcal{B}_0 and \mathcal{C}_0 deviate substantially from the perturbative expectations and \mathcal{B}_0 even comes out negative. However, as one would expect, r_m as well as the improvement parameters are closer to unity at the larger β value. The fits are discussed in more detail in Secs. VA and VB below.

TABLE II. Results of global fits to our AWI quark mass data according to Eqs. (56) and (57). The \mathcal{A} values were determined in Ref. [24]. In the cases where varying \mathcal{A} within its uncertainty had an effect, a second error is given to reflect the associated systematics.

β	χ^2/N_{DF}	Z	r_m	κ_{crit}	\mathcal{A} (no fit)	\mathcal{B}_0	\mathcal{C}_0	\mathcal{D}_0
3.4	32.1/9	0.8710(30)(10)	2.635(94)(5)	0.1369115(27)(1)	2.91(33)	-1.55(76)(1)	3.43(30)	10.0(9.1)(0.3)
3.55	26.2/10	0.9841(25)(3)	1.530(14)(1)	0.1371718(10)	2.27(14)	-0.81(45)(1)	1.89(25)(1)	1.2(1.2)

Repeating the $\beta = 3.4$ fit, excluding the lightest $m_s = m_\ell$ data point (rqcd017) as this was obtained on a small volume $LM_\pi = 3.2 < 4$, did not significantly impact on any of the fit parameters but resulted in increased errors in some cases: $r_m = 2.50(20)$, $\kappa_{\text{crit}} = 0.1369159(66)$ and $\mathcal{D}_0 = -0.7 \pm 17.0$. Note that the central value of \mathcal{D}_0 moved down by one standard deviation while the errors on r_m and κ_{crit} approximately doubled. Including the heavy rqcd019 point hardly affected any of the fit parameters, with the exception of $\mathcal{D}_0 = 16.5 \pm 4.4$, indicating a large positive value of this parameter. However, in view of the rather large improvement coefficients at $\beta = 3.4$, the rqcd019 results may very well be polluted by significant $\mathcal{O}(a^2)$ effects, which is why we chose to discard this point from further analysis.

IV. DETERMINATION OF THE PHYSICAL QUARK MASS VALUES

At each lattice spacing the average lattice quark mass m_{symm} for the $\bar{m} = m_{\text{symm}}$ trajectory is fixed by imposing a target value for the combination [7]

$$\begin{aligned} \phi_4 &\equiv 8t_0 \left(M_K^2 + \frac{1}{2} M_\pi^2 \right) \propto \bar{m} \\ &\propto \bar{m} + a \left[\frac{2d_m}{9} (m_s - m_\ell)^2 + (d_m + 3\tilde{d}_m) \bar{m}^2 \right] \\ &\quad + \mathcal{O}(a^2) \end{aligned} \quad (61)$$

at $\kappa_\ell = \kappa_s = \kappa_{\text{symm}}$, where t_0 is the gluonic scale defined in Ref. [29] and we have made use of the Gell-Mann–Oakes–Renner relation as well as of Eqs. (14) and (27). At the physical point the numerical value

$$\phi_{4,\text{ph}} = 1.117(38) \quad (62)$$

can be obtained from the pion and kaon masses in the electrically neutral isospin symmetric limit, $M_\pi = 134.8(3)$ MeV and $M_K = 494.2(4)$ MeV [32], and the result $\sqrt{8t_0} = 0.4144(59)(37)$ fm of the BMW Collaboration [30] for the continuum limit $N_f = 2 + 1$ theory. In the future we will independently determine a lattice scale and at that stage the value Eq. (62) may change.

The combination ϕ_4 will not vary strongly along the $\bar{m} = m_{\text{symm}}$ trajectory: At fixed renormalized quark masses ϕ_4 (and ϕ_2 defined below) can only be subject to $\mathcal{O}(a^2)$ lattice artefacts. This also holds when \bar{m} is varied as the effect of

the renormalization of the charge through b_g cancels from this combination. However, the proportionality of ϕ_4 to the average lattice quark mass \bar{m} is subject to order- a corrections, see Eqs. (14) and (61). The latter of the correction terms in Eq. (61) does not change along the $\bar{m} = m_{\text{symm}}$ line. The remaining $\mathcal{O}(a)$ correction term is proportional to $(m_s - m_\ell)^2$. On the continuum side, generalizing the Ademollo–Gatto theorem [33] and also as a consequence of the Gell-Mann–Okubo expansion [5,16,17], ϕ_4 cannot depend linearly on the symmetry breaking parameter $m_s - m_\ell$, i.e. it can only depend on $(M_K^2 - M_\pi^2)^2$ and higher powers. Indeed, to next-to-leading order $SU(3)$ ChPT [34,35] ϕ_4 is constant as long as \bar{m} is constant and it will only receive corrections at next-to-next-to-leading order [36]. Therefore, the $\bar{m} = m_{\text{symm}}$ line with $\phi_{4,\text{symm}} = \phi_{4,\text{ph}}$, where $\phi_{4,\text{symm}}$ refers to the ϕ_4 value at the point $m_s = m_\ell$, should go through the physical point, up to continuum and lattice effects that are both quartic in the pseudoscalar meson masses in units of the chiral symmetry breaking scale $4\pi F_0 \sim 1$ GeV. In view of these corrections that depend on $(M_K^2 - M_\pi^2)^2$ and ϕ_4 itself, we targeted a slightly larger value $\phi_{4,\text{symm}} \approx 1.15 > \phi_{4,\text{ph}}$, see Ref. [7].

In the overview plot Fig. 2 the positions of our analyzed ensembles in the ϕ_4 vs.

$$\phi_2 \equiv 8t_0 M_\pi^2 \propto \hat{m}_\ell \quad (63)$$

plane are shown, where at the physical point:

$$\phi_{2,\text{ph}} = 0.0801(28), \quad (64)$$

using again the physical values for t_0 and M_π from above. Abscissa and ordinate are approximately proportional to the light and average lattice quark masses, respectively. The physical target ranges $\phi_{4,\text{ph}}$ and $\phi_{2,\text{ph}}$ are shown as horizontal and vertical error bands. The line for $m_s = m_\ell$ corresponds to $\phi_4 = 3\phi_2/2$, for $\bar{m}_s = \bar{m}_{s,\text{ph}}$ we show a linear fit to the data while for $\bar{m} = m_{\text{symm}}$ we plot a constant plus quadratic function of $\phi_{2,\text{symm}} - \phi_2 \propto t_0(M_K^2 - M_\pi^2)$. Indeed, the ϕ_4 combination only mildly varies between the $\bar{m} = m_{\text{symm}}$ simulation points but changes significantly along the other two mass plane trajectories. The orange point at $\beta = 3.4$ corresponds to the ensemble D100 (see Table I) that does not enter any of our fits.

Along the $\bar{m} = m_{\text{symm}}$ trajectory order- a lattice artefacts as well as the leading continuum chiral correction both are

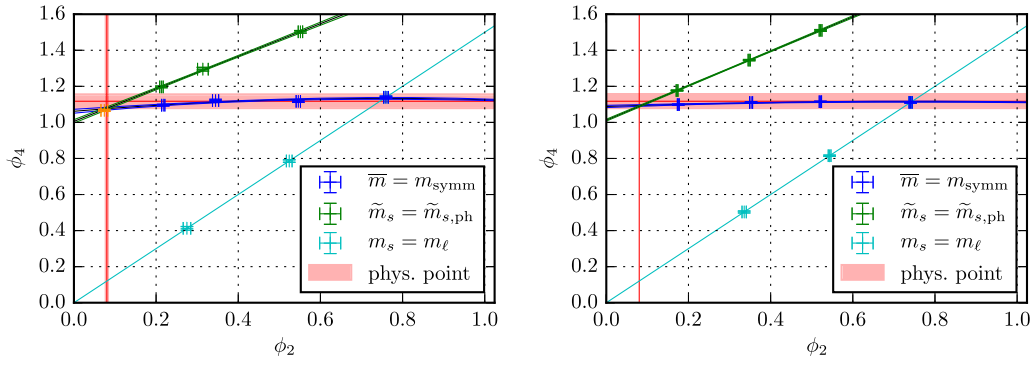


FIG. 2. Our simulation points in the $\phi_4 \sim \bar{m}$ [see Eq. (61)] vs. $\phi_2 \sim m_\ell$ [see Eq. (63)] plane. The bands correspond to the uncertainties of the physical point values Eqs. (62) and (64). $\phi_4 = (3/2)\phi_2$ along the $m_s = m_\ell$ line and the other curves represent fits to the data, including (tiny) error bands. Orange point: ensemble D100. The data points corresponding to ensembles rqcd019 and B250 are outside of the plotted range. Left: $\beta = 3.4$. Right: $\beta = 3.55$.

proportional to $(m_s - m_\ell)^2$. Because of this variation the target value at the $SU(3)$ symmetric point was deliberately chosen larger than its physical point estimate Eq. (62). At both couplings we have somewhat undershot this target value $\phi_{4,\text{symm}} = 1.15$: For our $\beta = 3.4$ and $\beta = 3.55$ data we obtain $\phi_{4,\text{symm}} = 1.139(6)$ and $\phi_{4,\text{symm}} = 1.111(4)$, respectively. This then results in smaller than physical central $\phi_{4,\text{ph}}$ values. From the fit to the $\bar{m} = m_{\text{symm}}$ points we find

$$\frac{\phi_{4,\text{ph}}}{\phi_{4,\text{symm}}} = 0.945(9), \quad \phi_{4,\text{ph}} = 1.076(8), \quad (65)$$

$$\frac{\phi_{4,\text{ph}}}{\phi_{4,\text{symm}}} = 0.985(6), \quad \phi_{4,\text{ph}} = 1.094(5), \quad (66)$$

at $\beta = 3.4$ and $\beta = 3.55$, respectively. In both cases the slope of ϕ_4 as a function of $(\phi_{2,\text{symm}} - \phi_2)^2$ is small but significant. It decreases toward the smaller lattice spacing, indicating that the main effect may be due to lattice artefacts. In hindsight, if we would have chosen

$\phi_{4,\text{symm}} \approx 1.18$ and $\phi_{4,\text{symm}} \approx 1.13$ at $\beta = 3.4$ and $\beta = 3.55$, respectively, we would have hit the central physical target value for ϕ_4 at $\phi_2 = \phi_{2,\text{ph}}$ along our $\bar{m} = m_{\text{symm}}$ line. Nevertheless, both extrapolated $\phi_{4,\text{ph}}$ values agree with the physical value $\phi_{4,\text{ph}} = 1.117(38)$ within errors. We remark that also this value is not final but depends on a future independent determination of the scale parameter t_0 .

In Fig. 3 we plot the ratio $\sqrt{t_0}/t_{0,\text{ph}}$ as a function of the light AWI quark mass ratio $\tilde{m}_\ell/\tilde{m}_{\ell,\text{ph}}$ where we normalize with respect to the corresponding physical mean values (see below). At both lattice spacings $\sqrt{t_0}$ along the $\bar{m} = m_{\text{symm}}$ line depends only mildly on m_ℓ but—as expected—it changes considerably along the other lines, and in particular along $m_s = m_\ell$. The dependence on the quark masses can be parametrized in terms of lattice spacing and continuum effects [35]. The latter are to leading order linear functions of $\bar{m} \propto \tilde{m}$ and $(\tilde{m}_s - \tilde{m}_\ell)^2 \propto (\hat{m}_s - \hat{m}_\ell)^2$, where the proportionalities hold up to tiny residual $\mathcal{O}(a)$ effects (see above). Extrapolating the $\bar{m} = m_{\text{symm}}$ data quadratically in $\tilde{m}_s - \tilde{m}_\ell \propto \bar{m} - \tilde{m}_\ell$, we obtain the physical point values

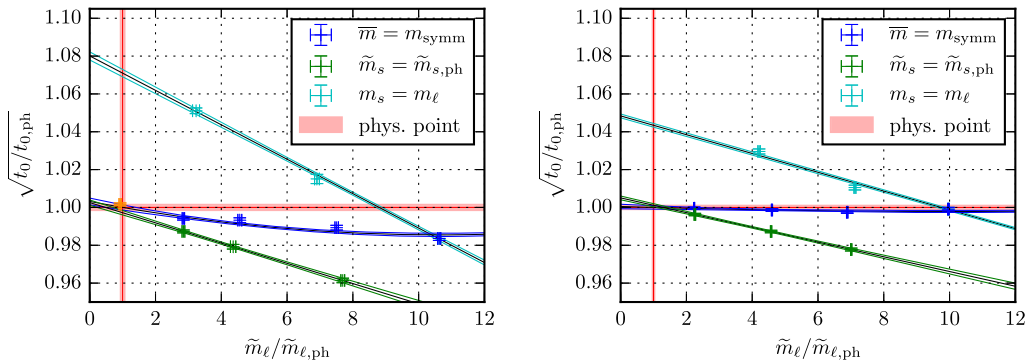


FIG. 3. $\sqrt{t_0}$ as a function of the AWI quark mass \tilde{m}_ℓ , normalized with respect to the extrapolated physical point values $\sqrt{t_{0,\text{ph}}}$ and $\tilde{m}_{\ell,\text{ph}}$, for our three quark mass plane trajectories. The lines are fits to the data. Orange point: ensemble D100. The data points corresponding to ensembles rqcd019 and B250 are outside of the plotted range. Left: $\beta = 3.4$. Right: $\beta = 3.55$.

$$\frac{\sqrt{t_{0,\text{ph}}}}{\sqrt{t_{0,\text{symm}}}} = 1.0167(18), \quad \frac{\sqrt{8t_{0,\text{ph}}}}{a} = 4.852(7), \quad (67)$$

$$\frac{\sqrt{t_{0,\text{ph}}}}{\sqrt{t_{0,\text{symm}}}} = 1.0009(13), \quad \frac{\sqrt{8t_{0,\text{ph}}}}{a} = 6.433(6), \quad (68)$$

for $\beta = 3.4$ and $\beta = 3.55$, respectively. Note that some of the t_0 values shown in the figure are preliminary, see Table I, and may have underestimated errors, due to very large autocorrelations times for this observable, that we may not yet have taken fully into account. Therefore, the $\sqrt{8t_{0,\text{ph}}}/a$ values quoted above should also be considered as preliminary. The curves shown in the figure are linear fits to the $\tilde{m}_s = \tilde{m}_{s,\text{ph}}$ and $m_s = m_\ell$ data and the constant plus quadratic fit in $\tilde{m} - \tilde{m}_\ell$ to the $\tilde{m} = m_{\text{symm}}$ data described above.

Note that linear lattice artefacts along the $m = m_s = m_\ell = \tilde{m}$ line are due to the change of the coupling $\tilde{g}^2 = (1 + b_g am)g^2$. This means that in this case the dependence on the lattice spacing a of the linear slope of $\sqrt{t_0(\hat{m})}$ as a function of m could serve to isolate the effect of b_g , when compared to the continuum limit mass dependence $t_{0,c}(\hat{m})$ along this line: From

$$\begin{aligned} a(\tilde{g}^2) &= \Lambda^{-1} \exp\left(-\frac{8\pi^2}{\beta_0 \tilde{g}^2} + \dots\right) \\ &= a(g^2)(1 + b_a am + \dots) \end{aligned} \quad (69)$$

it follows that $b_a = 8\pi^2 b_g / \beta_0 = 8\pi^2 b_g / 9$ for $N_f = 3$. This coefficient is related to the change of the slope

$$\begin{aligned} \frac{\sqrt{t_0(\hat{m})}}{\sqrt{t_0(0)}} &= \frac{a(g^2) \sqrt{t_{0,c}(\hat{m})}}{a(\tilde{g}^2) \sqrt{t_{0,c}(0)}} \\ &= (1 - b_a am) \frac{\sqrt{t_{0,c}(\hat{m})}}{\sqrt{t_{0,c}(0)}}. \end{aligned} \quad (70)$$

Note that $d_m + 3\tilde{d}_m$ and $Z_m r_m$ are required to relate $\sqrt{t_0(m)}$ to $\sqrt{t_0(\hat{m})}$. As the slope becomes more negative for the coarser lattice spacing, b_g must be positive, in agreement with the one-loop perturbative expectation [21]: A larger average quark mass results in a coarser effective lattice spacing.

As AWI masses can be determined more precisely than pseudoscalar masses and are less susceptible to finite volume effects, we will use these to set the physical quark masses, by imposing the FLAG value [32],

$$\frac{\tilde{m}_{\ell,\text{ph}}}{\tilde{m}_{\text{ph}}} \approx \frac{\hat{m}_{\ell,\text{ph}}}{\hat{m}_{\text{ph}}} = 0.1018(15), \quad (71)$$

to define the physical quark mass point. Also this target value may undergo a slight change in the future, once we have independently extrapolated the combination

$$\frac{3M_\pi^2}{2M_K^2 + M_\pi^2} = 0.1076(5) \quad (72)$$

to the continuum limit.

We remark that there are slight differences between ratios of renormalized and AWI quark masses \hat{m} and \tilde{m} , see Eq. (24). Since we keep \tilde{m} fixed along our main mass plane trajectory, the dependence on $\tilde{b}_P - \tilde{b}_A$ cancels from the ratio Eq. (71). However, a correction term

$$\begin{aligned} &a \frac{b_P - b_A}{3} (m_{\ell,\text{ph}} - m_{s,\text{ph}}) \\ &= a \frac{b_P - b_A}{3Z} (\tilde{m}_{\ell,\text{ph}} - \tilde{m}_{s,\text{ph}}) \end{aligned} \quad (73)$$

survives, see Eq. (24). Nonperturbatively, one finds [24] $b_P - b_A = 0.90(32)$ and $b_P - b_A = 0.59(14)$, respectively, at $\beta = 3.4$ and $\beta = 3.55$. At $\beta = 3.4$, where the above order- a correction is largest, using $Z^{-1} \approx 1.15$ and $a(\tilde{m}_{s,\text{ph}} - \tilde{m}_{\ell,\text{ph}}) \approx 0.023$ [see Table II and Eq. (75)], we obtain a change of about 0.8% from substituting the ratio of renormalized quark masses Eq. (71) by the ratio of AWI masses. This effect, that reduces to 0.4% at $\beta = 3.55$, is well below the 1.5% relative error of the FLAG average [32] that we use.

The global fit of Eqs. (56) and (57) to our mass data provides a parametrization of the AWI masses as functions of κ_ℓ and κ_s . The fit parameters can be found in Table II and the fit is discussed in detail in Secs. VA and VB below. At each lattice spacing we then determine the physical hopping parameter values $\kappa_{\ell,\text{ph}}$ and $\kappa_{s,\text{ph}}$ as well as the corresponding AWI masses $\tilde{m}_{\ell,\text{ph}}$ and $\tilde{m}_{s,\text{ph}}$ that satisfy Eq. (71) along the chiral trajectory $\tilde{m} = m_{\text{symm}}$. Note that since we have a parametrization of light and strange AWI masses as functions of the hopping parameters, we can also determine the physical point along any other chiral trajectory that incorporates it.⁴ Our procedure of finding the physical point is illustrated in Fig 4, where we plot this ratio as a function of κ_ℓ^{-1} . In addition to the $\tilde{m} = m_{\text{symm}}$ points (blue) that follow lines with little curvature, as expected from Eqs. (56) and (57), we also show the results of our subsequent measurements along the $\tilde{m}_s = \tilde{m}_{s,\text{ph}}$ trajectory (green), which nicely coincide with the parametrization, thereby validating our strategy. Note that the $m_s = m_\ell$ points (with the exception of the symmetric point on the $\tilde{m} = m_{\text{symm}}$ line) are not shown as the ratio displayed is trivial in this case. The error band of the target value is dominated by the uncertainty of Eq. (71).

⁴In the absence of an independent determination of the scale parameter t_0 , for the moment being we fix $\frac{1}{3} \sum_i \kappa_i^{-1} = 0.13675962$ and $\frac{1}{3} \sum_i \kappa_i^{-1} = 0.137$ at $\beta = 3.4$ and $\beta = 3.55$, respectively, i.e. we assume that our $\tilde{m} = m_{\text{symm}}$ curves go exactly through the physical point. As can be seen in Fig. 2 this assumption is justified. Along this line the physical point is then defined by Eq. (71).

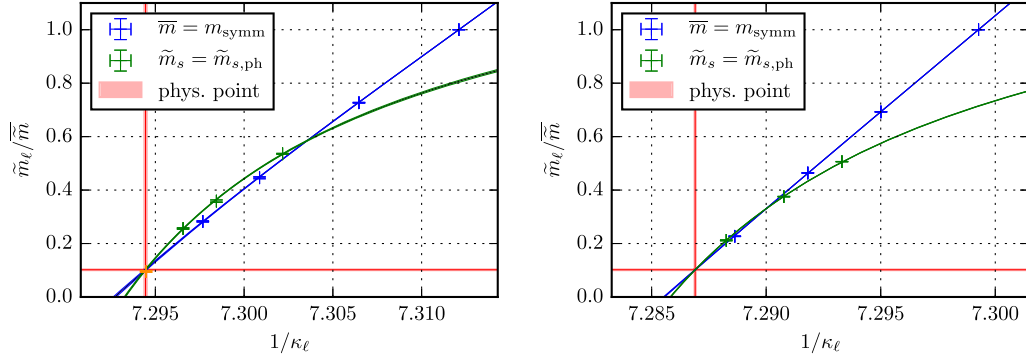


FIG. 4. Extrapolation of the AWI mass ratio \tilde{m}_ℓ/\tilde{m} of Eq. (71) to the physical point (horizontal and vertical bands). The curves correspond to Eqs. (56) and (57) with the parameter values of Table II. Orange point: ensemble D100. Left: $\beta = 3.4$. Right: $\beta = 3.55$.

The physical point values, postdicted including more statistics and the newly generated fixed AWI strange quark mass ensembles, read:

$$\kappa_{\ell,\text{ph}} = 0.1370906(13), \quad \kappa_{s,\text{ph}} = 0.1361024(25), \quad (74)$$

$$a\tilde{m}_{\ell,\text{ph}} = 0.000866(48), \quad a\tilde{m}_{s,\text{ph}} = 0.023780(65), \quad (75)$$

and

$$\kappa_{\ell,\text{ph}} = 0.1372326(5), \quad \kappa_{s,\text{ph}} = 0.1365373(10), \quad (76)$$

$$a\tilde{m}_{\ell,\text{ph}} = 0.000688(17), \quad a\tilde{m}_{s,\text{ph}} = 0.018887(28), \quad (77)$$

at $\beta = 3.4$ and $\beta = 3.55$, respectively. Our original targets had been $a\tilde{m}_{s,\text{ph}} = 0.0240$ at $\beta = 3.4$ and $a\tilde{m}_{s,\text{ph}} = 0.0189$ at $\beta = 3.55$. In the latter case this agrees with the corresponding value above. At $\beta = 3.4$, however, we mistuned by 1% since the estimate of c_A [19,37] changed during our study.

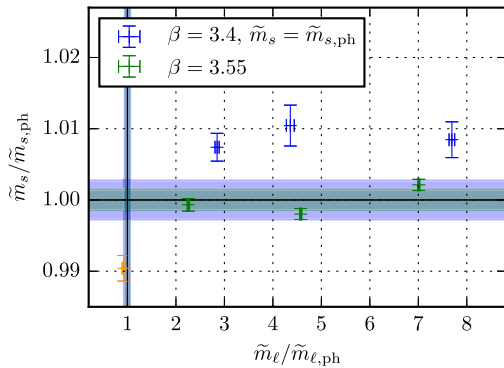


FIG. 5. The strange quark AWI masses along the $\tilde{m}_s = \tilde{m}_{s,\text{ph}}$ curves, normalized with respect to the (postdicted) central physical point values Eqs. (75) and (77), as a function of the corresponding light quark mass ratios. The error bands are dominated by the uncertainty of the target value Eq. (71), where we neglected the uncertainty of m_{symm} . Orange point: $\beta = 3.4$ ensemble D100.

In Fig. 5 we plot our measured AWI strange quark masses determined on the newly generated ensembles along the predicted $\tilde{m}_s = \tilde{m}_{s,\text{ph}}$ trajectory, normalized with respect to the postdicted values from the global fit shown in Eqs. (75) and (77) above as a function of the light quark AWI mass. Indeed, the two sets of AWI strange quark masses are constant within errors. The $\beta = 3.55$ data perfectly coincide with the expectation (see also the N204, N201 and D201 entries of Table I). The $\beta = 3.4$ data agree reasonably well with the original target value (see ensembles H107, H106 and C102 of Table I) but they are off by almost 3 standard deviations, corresponding to 1%, from the postdiction Eq. (75), that was obtained using an altered value of c_A [19].

Neglecting any uncertainty on $2m_\ell + m_s = 3m_{\text{symm}}$, the 1.5% error of the target range Eq. (71) translates into a small error on $\tilde{m}_{s,\text{ph}}$ and a larger relative error on $\tilde{m}_{\ell,\text{ph}}$. These uncertainties contribute to the horizontal and vertical error bands shown in the figure. Note that these would be wider if we could include a realistic error estimate for m_{symm} . The figure demonstrates that it is possible to tune the AWI strange quark mass to the desired value within a few per mille and even in the case where, due to the incomplete information on c_A , we mistuned to an incorrect target value the difference is extremely small.

V. DISCUSSION OF THE FITS AND THE RESULTING PARAMETERS

We will first investigate in more detail lattice spacing effects for the $\tilde{m} = m_{\text{symm}}$ and $m_s = m_\ell$ data, before presenting an overview of all AWI mass data, and discussing combinations of improvement coefficients.

A. $\tilde{m} = m_{\text{symm}}$ and $m_s = m_\ell$ data and improvement coefficients

Here we compare different projections of our quark mass data to the global fits Eqs. (56) and (57) with the parameter values shown in Table II.

In Fig. 6 we show the ratio of the AWI over the lattice quark mass $\tilde{m}/\tilde{m} = \tilde{m}/m$ as a function of \tilde{m} for our

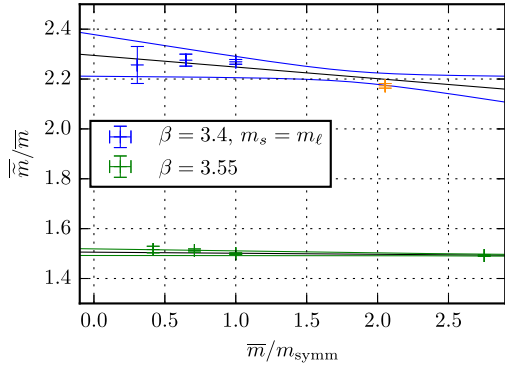


FIG. 6. The ratio of the AWI over the lattice quark mass along the $m_s = m_\ell$ trajectory, as a function of $\bar{m} = m_s = m_\ell$, normalized to the mass $m_{\text{symm}} \approx \bar{m}_{\text{ph}}$. The value of \bar{m}/\bar{m} at $\bar{m} = 0$ corresponds to the combination of renormalization constants Zr_m . Orange point: ensemble rqcd019 (excluded from the global fit). The curves correspond to Eq. (78), with the parameter values of Table II.

$m_s = m_\ell = m = \bar{m}$ data. Note that the right-most orange $\beta = 3.4$ point (rqcd019) did not enter the fit as we suspect this may be polluted by significant $\mathcal{O}(a^2)$ effects. To enable a direct comparison between different lattice spacings, the x-axis is normalized with respect to m_{symm} , the average lattice quark mass used along our $\bar{m} = m_{\text{symm}}$ trajectory. From Eq. (57) we can see that

$$\frac{\bar{m}}{\bar{m}} = Zr_m \left\{ 1 - a \left[\frac{\mathcal{C}_0 (m_s - m_\ell)^2}{9 \bar{m}} + \frac{\mathcal{D}_0}{2} \bar{m} \right] \right\}. \quad (78)$$

Therefore, we can directly read off the combination Zr_m at $\bar{m} = 0$ from the figure (as well as from Table II). Since the difference $m_s - m_\ell$ vanishes for the data shown, the slope corresponds to the combination $-Zr_m \mathcal{D}_0 a m_{\text{symm}}/2$. This becomes better constrained toward the larger β value but—as its effect is small—the deviation of this parameter from the tree-level expectation $\mathcal{D}_0 = 1$ is hard to extract. This also means that our results are quite insensitive regarding the value of \mathcal{D}_0 .

In Fig. 7 we show a combination that isolates the effect of $\mathcal{C}_0: \bar{m}$ over \bar{m}_{symm} as a function of $(m_s - m_\ell)^2$, normalized to the corresponding physical point value, for the constant average lattice quark mass data $\bar{m} = m_{\text{symm}}$. As the light quark mass decreases the ratio shown deviates from one. The parametrization can be read off from Eq. (78):

$$\frac{\bar{m}}{\bar{m}_{\text{symm}}} = 1 - \frac{\mathcal{C}_0 a (m_{s,\text{ph}} - m_{\ell,\text{ph}})^2}{9 m_{\text{symm}}} \left(\frac{m_s - m_\ell}{m_{s,\text{ph}} - m_{\ell,\text{ph}}} \right)^2. \quad (79)$$

This means the negative slope is proportional to \mathcal{C}_0 , which decreases considerably, increasing β from 3.4 to 3.55, see also Table II. For $\beta = 3.4$ we show the preliminary D100

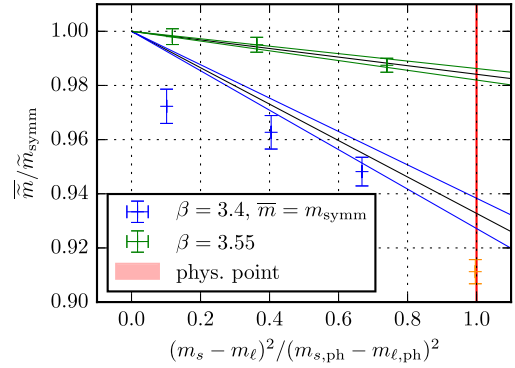


FIG. 7. The dependence of the average AWI quark mass on the difference of the lattice quark masses squared, along the $\bar{m} = m_{\text{symm}}$ trajectory. Orange point: ensemble D100. Both mass combinations are normalized with respect to their $m_s = m_\ell$ value \bar{m}_{symm} and their physical point value, respectively. The curves correspond to Eq. (79) with the parameter values of Table II.

physical point result (orange) that did not enter our global fit. The left-most point at $\beta = 3.4$ (corresponding to the H102 ensemble of Table I) exhibits the largest deviation of our data from the two global fits to data from 9 and 10 ensembles (15 and 16 quark mass values), respectively. Since $a\bar{m}$ is constant for all the $\beta = 3.4$ data shown in the figure and $a(m_s - m_\ell)$ is larger for the other points, we would not expect the average AWI quark mass on ensemble H102 to be particularly sensitive to higher order discretization effects. Therefore, we assume the deviation seen is a statistical fluctuation.

Finally, in Fig. 8 we show the ratio of AWI and lattice quark mass differences as a function of $m_s - m_\ell$ for the $\bar{m} = m_{\text{symm}}$ data. We normalize the ordinate with respect to its physical point value, to enable comparison between different lattice spacings. We also display the global fits. Note that the right-most orange $\beta = 3.4$ point (D100) did not enter the fit as we regard its error as unreliable, due to limited statistics. From Eq. (56) we see that

$$\frac{\bar{m}_s - \bar{m}_\ell}{m_s - m_\ell} = Z \left\{ 1 - a \left[\frac{\mathcal{A}}{6} (m_s - m_\ell) + \mathcal{B}_0 \bar{m} \right] \right\}. \quad (80)$$

Therefore, at $m_s = m_\ell$ we can read off the combination $Z(1 - \mathcal{B}_0 a m_{\text{symm}})$. This is somewhat larger than the Z parameters that are listed in Table II because \mathcal{B}_0 is negative in both cases. The slope corresponds to $-Z\mathcal{A}a(m_{s,\text{ph}} - m_{\ell,\text{ph}})/6$. Note that the value of the parameter \mathcal{A} that was obtained independently [24] is consistent with our data.

We have demonstrated that \mathcal{A} , \mathcal{C}_0 and \mathcal{D}_0 can be constrained from data along the $\bar{m} = m_{\text{symm}}$ and $m_s = m_\ell$ lines. While the sensitivity to \mathcal{D}_0 is small, \mathcal{B}_0 cannot be constrained at all from data points along these two lines. Obviously, \bar{m} needs to be varied for $m_s \neq m_\ell$ for the results

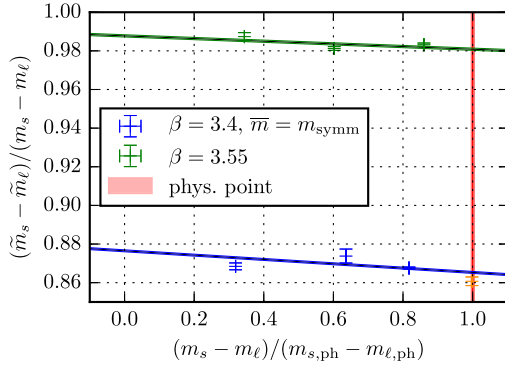
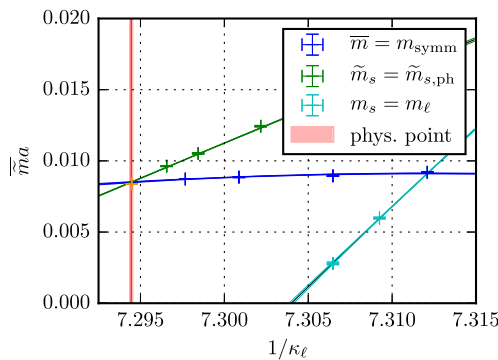


FIG. 8. The ratio between AWI and lattice quark mass differences along the $\bar{m} = m_{\text{symm}}$ trajectory, as a function of $m_s - m_\ell$, normalized to this mass difference at the physical point. Orange point: ensemble D100. Up to an order- a term, the value of the ratio at $m_s - m_\ell = 0$ corresponds to the renormalization constant combination Z . The curves correspond to Eq. (80) with the parameter values of Table II.

to become sensitive to \mathcal{B}_0 . Unfortunately, to enable a precise determination of Z [and of $r_m = (Zr_m)/Z$] some knowledge of \mathcal{B}_0 is required but we were only able to constrain \mathcal{B}_0 , once data points from other regions of the quark mass plane were added, in our case along the $\tilde{m}_s = \tilde{m}_{s,\text{ph}}$ line. Another possibility of achieving this would have been to follow a partially quenched strategy, computing valence quark AWI masses along the sea quark symmetric line $m_s = m_\ell$. Nevertheless, in order to determine the $\tilde{m}_s = \tilde{m}_{s,\text{ph}}$ line from the two chiral trajectories $\bar{m} = m_{\text{symm}}$ and $m_s = m_\ell$ there is no need for a very accurate value of \mathcal{B}_0 since the $\mathcal{B}_0 a m_{\text{symm}}$ contribution to Z only amounts to a 0.6% correction, even on the coarser $\beta = 3.4$ ensemble.

B. AWI and pseudoscalar mass data

In Fig. 9 we plot the average AWI mass in lattice units as a function of κ_ℓ^{-1} for our three quark mass plane trajectories: $\bar{m} = m_{\text{symm}}$, $\tilde{m}_s = \tilde{m}_{s,\text{ph}}$ and $m_s = m_\ell$. The curves correspond to our fit according to Eq. (57) with parameters as



shown in Table II. The $\bar{m} = m_{\text{symm}}$ curve is almost constant as along this line \bar{m} only changes due to an $\mathcal{O}(a)$ term that is parametrized by \mathcal{C}_0 , see Fig. 7. The curvature is not visible on the scale of Fig. 9.

In Fig. 10 a comparison is shown between strange and light AWI mass differences $\tilde{m}_s - \tilde{m}_\ell$ and the fit Eq. (56). In this representation the $m_s = m_\ell$ points obviously coincide with zero and are therefore not shown. Overall, we have good coverage of the quark mass plane and the data are described reasonably well by the fit. Like in Fig. 9, at both lattice spacings that we investigated, the $\bar{m} = m_{\text{symm}}$ and $\tilde{m}_s - \tilde{m}_{s,\text{ph}}$ curves intersect very close to (and in statistical agreement with) the preferred position of the physical point.

Finally, in Fig. 11 we display the ratio $3M_\pi^2/(2M_K^2 + M_\pi^2)$ as a function of $8t_{0,\text{ph}}M_\pi^2$ for the $\bar{m} = m_{\text{symm}}$ and $\tilde{m}_s = \tilde{m}_{s,\text{ph}}$ trajectories. Again, $t_{0,\text{ph}}$ denotes the value of this parameter at the physical point, which is somewhat larger than its value $t_{0,\text{symm}}$ at the $SU(3)$ flavor symmetric point, see Fig. 3 and Eqs. (67) and (68). The curves shown correspond to the parametrizations

$$\frac{3M_\pi^2}{2M_K^2 + M_\pi^2} = \frac{3M_\pi^2}{\alpha M_\pi^2 + (3 - \alpha)M_{\pi,\text{symm}}^2}, \quad (81)$$

$$\frac{3M_\pi^2}{2M_K^2 + M_\pi^2} = \frac{3M_\pi^2}{\gamma/(8t_{0,\text{ph}}) + 2M_\pi^2}, \quad (82)$$

for $\bar{m} = m_{\text{symm}}$ and $\tilde{m}_s = \tilde{m}_{s,\text{ph}}$, respectively. The functional dependencies enforce the first curve to take the value one at the symmetric point and both curves to go through zero for $M_\pi = 0$. For the above ratio of pseudoscalar masses we expect to find the value 0.1076(5) [the horizontal band, see Eq. (72)] at the physical point, which is defined through $8t_{0,\text{ph}}M_{\pi,\text{ph}}^2 = \phi_{2,\text{ph}} = 0.0801(28)$ [the vertical band, see Eq. (64)].

The dimensionless fit parameters can be related to meson masses at the symmetric and physical points:

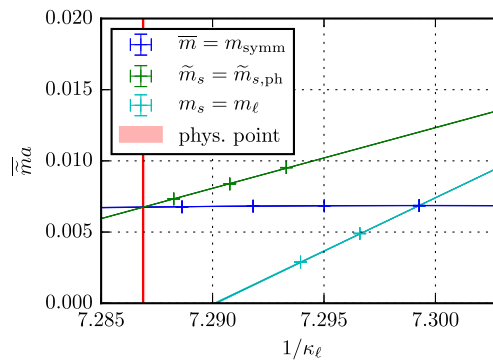


FIG. 9. The average AWI quark mass along our three trajectories, together with the fit according to Eq. (57) with the parameter values of Table II vs. κ_ℓ^{-1} . Orange point: ensemble D100. Left: $\beta = 3.4$. Right: $\beta = 3.55$.

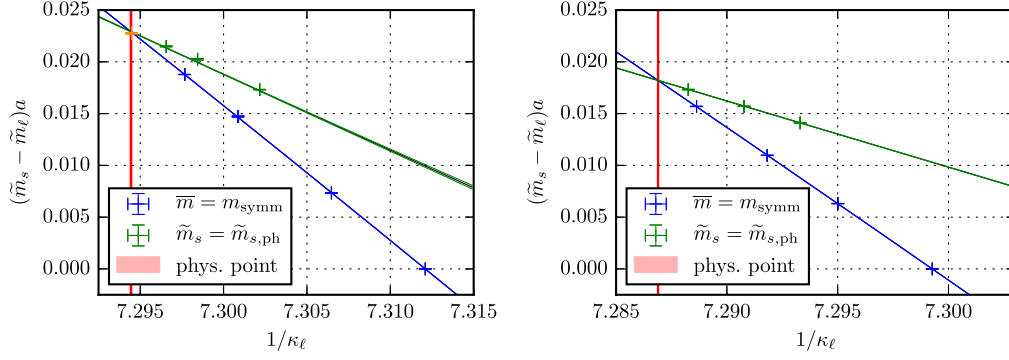


FIG. 10. Differences between AWI quark masses, together with the fit according to Eq. (56) with the parameter values of Table II vs. κ_ℓ^{-1} . Orange point: ensemble D100. Left: $\beta = 3.4$. Right: $\beta = 3.55$.

$$\alpha = \frac{2M_{K,\text{ph}}^2 + M_{\pi,\text{ph}}^2 - 3M_{\pi,\text{symm}}^2}{M_{\pi,\text{ph}}^2 - M_{\pi,\text{symm}}^2}, \quad (83)$$

$$\gamma = 8t_{0,\text{ph}}(2M_{K,\text{ph}}^2 - M_{\pi,\text{ph}}^2) = 2(\phi_{4,\text{ph}} - \phi_{2,\text{ph}}). \quad (84)$$

The fitted parameter values read

$$\alpha = 0.235(19), \quad \gamma = 2.054(12), \quad (85)$$

$$\alpha = -0.025(15), \quad \gamma = 2.062(6), \quad (86)$$

for $\beta = 3.4$ and $\beta = 3.55$, respectively. Both γ values agree well with the physical point expectation $2(\phi_{4,\text{ph}} - \phi_{2,\text{ph}}) = 2.075(70)$. The curvature of the $\bar{m} = m_{\text{symm}}$ line is of a higher order in ChPT and also subject to an $\mathcal{O}(a)$ lattice effect. The change of the parameter α with β indicates that the latter dominates.

At the physical point we obtain the following values for the ratio Eq. (72) from the fits Eqs. (81)–(82): 0.1087(6)(37) and 0.1086(6)(35) for the $\bar{m} = m_{\text{symm}}$ and $\tilde{m}_s = \tilde{m}_{s,\text{ph}}$ data, respectively, at $\beta = 3.4$ and 0.1074(4)(37) and 0.1082(3)(35) at $\beta = 3.55$. The first errors are statistical only while the second errors given include the propagation of the uncertainty of $\phi_{2,\text{ph}}$ that defines the

physical point, which is dominated by the scale uncertainty of t_0 . Just considering the statistical errors and taking the central value of $\phi_{2,\text{ph}}$ for granted, all ratios agree reasonably well with the “experimental” value 0.1076(5) quoted in Eq. (72): Imposing the continuum FLAG ratio [32] Eq. (71) of renormalized quark masses gives the expected result for this ratio of experimental pseudoscalar masses, also at our two finite lattice spacings. It is particularly reassuring that this is the case independent of the quark mass trajectory. This should allow us to improve on the precision of present quark mass determinations, once more lattice spacings are analysed and the continuum limit has been taken.

C. Further combinations of improvement coefficients

We have determined the combinations of improvement coefficients Eqs. (32)–(34) as well as r_m , the ratio of the singlet over nonsinglet quark mass renormalization constants, see Table II. Additional information on $\mathcal{A} = b_P - b_A - 2b_m$, $b_P - b_A$ and b_m exists from Ref. [24]. Using these results, we can estimate other improvement coefficients: From Eq. (33) we infer that

$$d_m = -\frac{1}{4} \left(2\mathcal{C}_0 + \frac{b_P - b_A}{r_m} \right). \quad (87)$$

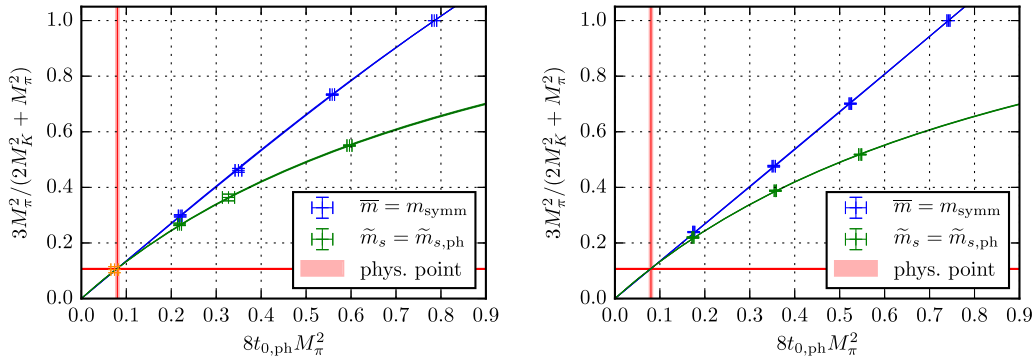


FIG. 11. The ratio $3M_\pi^2 / (2M_K^2 + M_\pi^2)$ as a function of $8t_{0,\text{ph}}M_\pi^2$ along the $\bar{m} = m_{\text{symm}}$ and $\tilde{m}_s = \tilde{m}_{s,\text{ph}}$ mass plane trajectories for our two lattice spacings. The vertical and horizontal bands correspond to the physical point. The parametrization of the fit curves is given in Eqs. (81) and (82). Orange point: ensemble D100. Left: $\beta = 3.4$. Right: $\beta = 3.55$.

TABLE III. Various improvement coefficient (combinations). \mathcal{A} , \mathcal{B}_0 , \mathcal{C}_0 and \mathcal{D}_0 are listed in Table II. The b_m and $b_P - b_A$ values below have been obtained in Ref. [24].

Coefficient	Perturbation theory	$\beta = 3.4$	$\beta = 3.55$
b_m	$-1/2 - 0.0703g^2$	-1.04(31)	-0.85(14)
d_m	$-1/2 - 0.0703g^2$	-1.80(16)	-1.04(13)
$b_P - b_A$	$0.0012g^2$	0.90(32)	0.59(14)
$\tilde{b}_m + \tilde{b}_P - \tilde{b}_A$	$\mathcal{O}(g^4)$	0.12(51)	0.34(21)
$\tilde{d}_m - \tilde{b}_m$	$\mathcal{O}(g^4)$	-1.5(1.5)	-0.39(27)

Equation (32) gives

$$\tilde{b}_m + \tilde{b}_P - \tilde{b}_A = -\frac{1}{3}[\mathcal{B}_0 + (r_m + 1)(b_P - b_A) + 2b_m]. \quad (88)$$

Then from the above and Eq. (34) we obtain

$$\tilde{d}_m - \tilde{b}_m = \frac{1}{12} \left[4\mathcal{B}_0 + 2\mathcal{C}_0 - 2\mathcal{D}_0 + \frac{1 + 4r_m^2}{r_m} (b_P - b_A) + 8b_m \right]. \quad (89)$$

We collect the resulting estimates in Table III. Like \mathcal{A} , \mathcal{B}_0 , \mathcal{C}_0 , \mathcal{D}_0 and r_m displayed in Table II, also these parameters appear to converge toward the perturbative expectations as the lattice spacing is reduced. In particular $d_m \approx b_m$ holds at $\beta = 3.55$.

VI. SUMMARY AND OUTLOOK

We outlined a strategy to keep the strange quark mass, determined through the axial Ward identity, constant in simulations with $N_f = 2 + 1$ flavors of Wilson fermions, implementing full order- a improvement, see Eqs. (39), (41) and (47). This was successfully tested to very high precision at two lattice spacings, $a \approx 0.085$ fm and $a \approx 0.064$ fm, see Fig. 5. We estimated this procedure to differ, due to as yet only partially known flavor singlet $\mathcal{O}(a)$ effects, from keeping the renormalized strange quark mass constant by less than one percent, even at the coarser lattice spacing. Furthermore, we worked out how valence quark hopping parameters need to be adjusted, see Sec. II D. This will be used in future studies of charm physics.

We computed several combinations of renormalization constants and order- a improvement coefficients, see Tables II and III. We observed that the parameters that are either related to flavor singlet quark mass combinations (\tilde{b}_m , \tilde{b}_P , \tilde{b}_A), flavor singlet currents (r_m , d_m) or both (\tilde{d}_m) come out very different from the corresponding perturbative expectations. However, these seem to converge rapidly in the direction of the tree-level results when increasing $\beta = 6/g^2$ from 3.4 to 3.55. Nonperturbative order- a improvement of all currents of interest is ongoing, see, e.g., Refs. [19,24].

In order to set the physical strange quark mass we also determined the physical point in the κ_s^{-1} vs. κ_ℓ^{-1} plane. Its position may still undergo changes in the future, once the continuum limit has been taken independently, which then might necessitate a slight reweighting [38,39] of the strange quark mass. Having ensembles along three lines in the quark mass plane ($2m_\ell + m_s = 3m_{\text{symm}}$, $\tilde{m}_s = \tilde{m}_{s,\text{ph}}$ and $m_s = m_\ell$) enables tests of the convergence of $SU(2)$ and $SU(3)$ ChPT and of expansions in the $SU(3)$ symmetry breaking parameter [5] as well as highly constrained physical point extrapolations. It also allows us to pursue a nonperturbative renormalization and order- a improvement program.

Results on baryon distribution amplitudes along the $2m_\ell + m_s = \text{const}$ trajectory at one lattice spacing have already been published [40]. Further results on distribution amplitudes, also utilizing the constant strange quark mass points, are in preparation and an article on light hadron spectroscopy is forthcoming.

ACKNOWLEDGMENTS

This work was supported by the Deutsche Forschungsgemeinschaft Grant No. SFB/TRR 55. The authors gratefully acknowledge the Gauss Centre for Supercomputing e.V. (<http://www.gauss-centre.eu>) for granting computer time on SuperMUC at Leibniz Supercomputing Centre (LRZ, <http://www.lrz.de>) and JUQUEEN at Jülich Supercomputing Center (JSC, <http://www.fz-juelich.de/ias/jsc>). GCS is the alliance of the three national supercomputing centers HLRS (Universität Stuttgart), JSC (Forschungszentrum Jülich) and LRZ (Bayerische Akademie der Wissenschaften), funded by the German Federal Ministry of Education and Research (BMBF) and the German State Ministries for Research of Baden-Württemberg (MWK), Bayern (StMWFK) and Nordrhein-Westfalen (MIWF). The authors also gratefully acknowledge computer time provided by PRACE (Partnership for Advanced Computing in Europe, <http://www.prace-ri.eu>) as part of the project ContQCD. Additional simulations were performed on the Regensburg iDataCool cluster and on the SFB/TRR 55 QPACE computer [41,42]. OPENQCD [43,44] was used to generate the main gauge ensembles, as part of the joint CLS effort [7]. Additional $m_s = m_\ell$ ensembles were generated on QPACE (using BQCD [42,45]) and on the Wilson HPC Cluster at IKP Mainz. Two-point functions were computed using the CHROMA [46] software package, along with the locally deflated domain decomposition solver implementation of OPENQCD [43]. We thank Christian Hoelbling for his permission to reproduce a figure of Ref. [1]. We thank Mattia Bruno, Sara Collins, Piotr Korcyl and Rainer Sommer for discussions, Tassos Vladikas for useful comments relating to an earlier draft, Benjamin Gläbke for software support, Fabian Hutzler for the generation of some of the two-point functions and all our other CLS colleagues.

- [1] C. Hoelbling, Lattice QCD: concepts, techniques and some results, *Acta Phys. Pol. B* **45**, 2143 (2014).
- [2] C. Hoelbling, Light hadron spectroscopy and pseudoscalar decay constants, Proc. Sci., LATTICE2010 (2010) 011 [arXiv:1102.0410].
- [3] Z. Fodor and C. Hoelbling, Light hadron masses from Lattice QCD, *Rev. Mod. Phys.* **84**, 449 (2012).
- [4] W. Bietenholz *et al.* (QCDSF and UKQCD Collaborations), Tuning the strange quark mass in lattice simulations, *Phys. Lett. B* **690**, 436 (2010).
- [5] W. Bietenholz *et al.* (QCDSF and UKQCD Collaborations), Flavour blindness and patterns of flavour symmetry breaking in lattice simulations of up, down and strange quarks, *Phys. Rev. D* **84**, 054509 (2011).
- [6] T. Inoue, S. Aoki, T. Doi, T. Hatsuda, Y. Ikeda, N. Ishii, K. Murano, H. Nemura, and K. Sasaki (HAL QCD Collaboration), Two-baryon potentials and H-dibaryon from 3-flavor Lattice QCD simulations, *Nucl. Phys. A* **881**, 28 (2012).
- [7] M. Bruno *et al.* (CLS), Simulation of QCD with $N_f = 2 + 1$ flavors of non-perturbatively improved Wilson fermions, *J. High Energy Phys.* **02** (2015) 043.
- [8] T. Blum *et al.* (RBC and UKQCD Collaborations), Domain Wall QCD with physical quark masses, *Phys. Rev. D* **93**, 074505 (2016).
- [9] S. Aoki, G. Cossu, X. Feng, S. Hashimoto, T. Kaneko, J.-I. Noaki, and T. Onogi (JLQCD Collaboration), Light meson electromagnetic form factors from three-flavor lattice QCD with exact chiral symmetry, *Phys. Rev. D* **93**, 034504 (2016).
- [10] K. Orginos, A. Parreño, M. J. Savage, S. R. Beane, E. Chang, and W. Detmold (NPLQCD Collaboration), Two nucleon systems at $m_\pi \sim 450$ MeV from lattice QCD, *Phys. Rev. D* **92**, 114512 (2015).
- [11] K.-I. Ishikawa, N. Ishizuka, Y. Kuramashi, Y. Nakamura, Y. Namekawa, Y. Taniguchi, N. Ukita, T. Yamazaki, and T. Yoshie (PACS Collaboration), 2 + 1 flavor QCD simulation on a 96^4 lattice, Proc. Sci., LATTICE2015 (2016) 075, [arXiv:1511.09222].
- [12] B. Yoon *et al.* (NME Collaboration), Controlling excited-state contamination in nucleon matrix elements, *Phys. Rev. D* **93**, 114506 (2016).
- [13] G. Herdoíza, K. Jansen, C. Michael, K. Ottnad, and C. Urbach, Determination of low-energy constants of Wilson chiral perturbation theory, *J. High Energy Phys.* **05** (2013) 038.
- [14] A. Bazavov *et al.* (Fermilab Lattice and MILC Collaborations), Charmed and light pseudoscalar meson decay constants from four-flavor lattice QCD with physical light quarks, *Phys. Rev. D* **90**, 074509 (2014).
- [15] S. Borsányi *et al.* (BMW-c), *Ab initio* calculation of the neutron-proton mass difference, *Science* **347**, 1452 (2015).
- [16] M. Gell-Mann, Symmetries of baryons and mesons, *Phys. Rev.* **125**, 1067 (1962).
- [17] S. Okubo, Note on unitary symmetry in strong interactions, *Prog. Theor. Phys.* **27**, 949 (1962).
- [18] T. Bhattacharya, R. Gupta, W. Lee, S. R. Sharpe, and J. M. S. Wu, Improved bilinears in Lattice QCD with non-degenerate quarks, *Phys. Rev. D* **73**, 034504 (2006).
- [19] J. Bulava, M. D. Morte, J. Heitger, and C. Wittmeier (ALPHA Collaboration), Non-perturbative improvement of the axial current in $N_f = 3$ Lattice QCD with Wilson fermions and tree-level improved gauge action, *Nucl. Phys. B* **896**, 555 (2015).
- [20] J. Bulava, M. D. Morte, J. Heitger, and C. Wittmeier (ALPHA Collaboration), Non-perturbative renormalization of the axial current in $N_f = 3$ lattice QCD with Wilson fermions and tree-level improved gauge action, *Phys. Rev. D* **93**, 114513 (2016).
- [21] M. Lüscher, S. Sint, R. Sommer, and P. Weisz, Chiral symmetry and $O(a)$ improvement in Lattice QCD, *Nucl. Phys. B* **478**, 365 (1996).
- [22] Y. Taniguchi and A. Ukawa, Perturbative calculation of improvement coefficients to $O(g^2a)$ for bilinear quark operators in Lattice QCD, *Phys. Rev. D* **58**, 114503 (1998).
- [23] M. Constantinou, R. Horsley, H. Panagopoulos, H. Perlt, P. E. L. Rakow, G. Schierholz, A. Schiller, and J. M. Zanotti, Renormalization of local quark-bilinear operators for $N_f = 3$ flavors of stout link nonperturbative clover fermions, *Phys. Rev. D* **91**, 014502 (2015).
- [24] P. Korcyl and G. S. Bali, Non-perturbative determination of improvement coefficients using coordinate space correlators in $N_f = 2 + 1$ lattice QCD, arXiv:1607.07090.
- [25] M. Constantinou, M. Hadjiantonis, and H. Panagopoulos, Renormalization of flavor singlet and nonsinglet fermion bilinear operators, Proc. Sci., LATTICE2014 (2014) 298, [arXiv:1411.6990].
- [26] Stefan Sint and Peter Weisz, Further results on $O(a)$ improved Lattice QCD to one loop order of perturbation theory, *Nucl. Phys. B* **502**, 251 (1997).
- [27] S. Sint and P. Weisz, Further one loop results in $O(a)$ improved Lattice QCD, *Nucl. Phys. B, Proc. Suppl.* **63**, 856 (1998).
- [28] P. Fritzsche, F. Knechtli, B. Leder, M. Marinkovic, S. Schaefer, R. Sommer, and F. Virotta (ALPHA Collaboration), The strange quark mass and Lambda parameter of two flavor QCD, *Nucl. Phys. B* **865**, 397 (2012).
- [29] M. Lüscher, Properties and uses of the Wilson flow in Lattice QCD, *J. High Energy Phys.* **08** (2010) 071; **03** (2014) 092(E).
- [30] S. Borsányi *et al.* (BMW-c), High-precision scale setting in Lattice QCD, *J. High Energy Phys.* **09** (2012) 010.
- [31] M. Lüscher and S. Schaefer, Lattice QCD without topology barriers, *J. High Energy Phys.* **07** (2011) 036.
- [32] S. Aoki *et al.* (FLAG), Review of lattice results concerning low-energy particle physics, *Eur. Phys. J. C* **74**, 2890 (2014).
- [33] M. Ademollo and R. Gatto, Nonrenormalization Theorem for the Strangeness Violating Vector Currents, *Phys. Rev. Lett.* **13**, 264 (1964).
- [34] J. Gasser and H. Leutwyler, Chiral perturbation theory: Expansions in the mass of the strange quark, *Nucl. Phys. B* **250**, 465 (1985).
- [35] O. Bär and M. Golterman, Chiral perturbation theory for gradient flow observables, *Phys. Rev. D* **89**, 034505 (2014); **89**, 099905(E) (2014).
- [36] G. Amorós, J. Bijnens, and P. Talavera, Two point functions at two loops in three flavor chiral perturbation theory, *Nucl. Phys. B* **568**, 319 (2000).
- [37] J. Bulava, M. D. Morte, J. Heitger, and C. Wittmeier (ALPHA Collaboration), Determination of c_A in three-

- flavour Lattice QCD with Wilson fermions and tree-level improved gauge action, Proc. Sci., LATTICE2013 (2014) 311, [arXiv:1312.3591].
- [38] J. Finkenrath, F. Knechtli, and B. Leder, One flavor mass reweighting in Lattice QCD, Nucl. Phys. **B877**, 441 (2013); **B880**, 574(E) (2014).
- [39] B. Leder and J. Finkenrath, Tuning of the strange quark mass with optimal reweighting, Proc. Sci., LATTICE2014 (2015) 040, [arXiv:1501.06617].
- [40] G. S. Bali *et al.* (RQCD Collaboration), Light-cone distribution amplitudes of the baryon octet, J. High Energy Phys. **02** (2016) 070.
- [41] H. Baier *et al.*, QPACE: A QCD parallel computer based on Cell processors, Proc. Sci., LAT2009 (2009) 001, [arXiv:0911.2174].
- [42] Y. Nakamura, A. Nobile, D. Pleiter, H. Simma, T. Streuer, T. Wettig, and F. Winter, Lattice QCD applications on QPACE, Procedia Computer Science **4**, 841 (2011).
- [43] <http://luscher.web.cern.ch/luscher/openQCD/>.
- [44] M. Lüscher and S. Schaefer, Lattice QCD with open boundary conditions and twisted-mass reweighting, Comput. Phys. Commun. **184**, 519 (2013).
- [45] Y. Nakamura and H. Stüben, BQCD—Berlin quantum chromodynamics program, Proc. Sci., LATTICE2010 (2010) 011, [arXiv:1102.0410].
- [46] R. G. Edwards and B. Joó (SciDAC, LHP Collaboration and UKQCD Collaboration), The Chroma software system for Lattice QCD, Nucl. Phys. B Proc. Suppl. **140**, 832 (2005).